INTERNATIONAL ATOMIC ENERGY AGENCY
UNITED NATIONS EDUCATIONAL, SCIENTIFIC AND CULTURAL ORGANIZATION

INTERNATIONAL CENTRE FOR THEORETICAL PHYSICS
34100 TRIESTE (ITALY) - P.O.B. 586 - MIRAMARE - STRADA COSTIERA 11 - TELEPHONES: 224281/9/240/0
CABLE: CENTRATOM - TELEX 460392-1

SMR/115 - 24

WINTER COLLEGE ON LASERS, ATOMIC AND MOLECULAR PHYSICS

(21 January - 22 March 1985)

TYPES OF LASERS

O. SVELTO
Centro di Elettronica Quantistica
e Strumentazione Elettronica
Istituto di Fisica del Politecnico
Piazza Leonardo da Vinci, 32
20133 Milano
Italy

6

Types of Lasers

6.1 INTRODUCTION

This chapter contains miscellaneous data and practical information about a number of lasers. It should be pointed out that there are many more lasers in existence than just those described here. This chapter, however, concentrates on those types which are most commonly used and whose characteristics are representative of a whole category of lasers. It should also be noted that some of the data presented in this chapter (for example, on output powers and energies) are likely to be rapidly superseded. These data are, therefore, presented only as a rough guide.

We will consider the following types of lasers: (1) solid-state (crystal or glass) lasers, (2) gas lasers, (3) dye lasers, (4) chemical lasers, (5) semiconductor lasers, (6) color-center lasers, and (7) free-electron lasers.

6.2 SOLID-STATE LASERS

The term solid-state laser is usually reserved for those lasers having as their active medium either an insulating crystal or a glass. Semiconductor lasers will be considered in a separate section since the mechanisms for pumping and for laser action are quite different. Solid-state lasers often use as their active species impurity ions introduced into an ionic crystal. Usually the ion belongs to one of the series of transition elements in the periodic table (e.g., transition metal ions, notably Cr^{3+}, or rare earth ions, notably Nd^{3+} or Ho^{3+}). The transitions used for laser action involve states

belonging to the inner unfilled shells. These transitions are therefore not so strongly influenced by the crystal field. This in turn means that the transitions are quite sharp (i.e., σ reasonably large) and the nonradiative channels are fairly weak (i.e., τ reasonably long). Consequently the threshold pump rate ($W_p \propto 1/\sigma\tau$ for a four-level laser) is low enough to allow laser action.

6.2.1 *The Ruby Laser*[1]

This type of laser was the first to be made to operate,[2,3] and still continues to be used. Ruby, which has been known for hundreds of years as a naturally occurring precious stone, is a crystal of Al_2O_3 (corundum) in which some of the Al^{3+} ions are replaced by Cr^{3+} ions. As a laser material, it is usually obtained by crystal growth from a molten mixture of Cr_2O_3 (~0.05% by weight) and Al_2O_3. The laser energy levels are those of the Cr^{3+} ion in the Al_2O_3 lattice, and the main levels of interest are indicated in Fig. 6.1. Laser action usually occurs on the $\bar{E} \rightarrow {}^4A_2$ transition (R_1 line, $\lambda_1 \simeq 694.3$ nm, red). Ruby has two main pump bands ${}^4F_1$ and ${}^4F_2$ centered at wavelengths of 0.55 μm (green) and 0.42 μm (violet), respectively. These bands are connected by a fast ($\sim 10^{-7}$ s) nonradiative decay to both $2\bar{A}$ and $\bar{E}$ states. Since these last two states are also connected to each other by a very fast nonradiative decay ($\sim 10^{-9}$ s), thermalization of their population occurs which results in the $\bar{E}$ level being the more heavily populated. The frequency separation between $2\bar{A}$ and $\bar{E}$ (~ 29 cm^{-1}) is small compared to (kT/h), and the $2\bar{A}$ population is comparable with the $\bar{E}$ level population. It is thus possible to obtain laser action on the $2\bar{A} \rightarrow {}^4A_2$ transition also (R_2 line, $\lambda_2 \simeq 0.6928$ μm) by using, for instance, the dispersive systems of Fig. 5.7. Despite the complication of having these two laser transitions, it is apparent that ruby operates as a three-level laser.

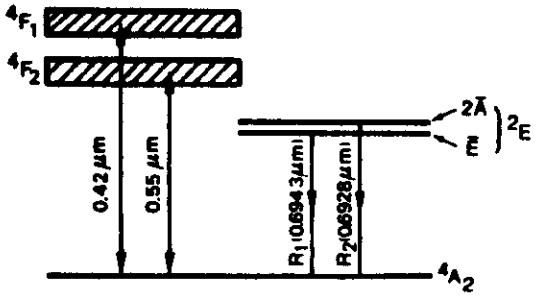

FIG. 6.1. Energy levels of ruby.

As already discussed in connection with Fig. 2.14, the R_1 transition is predominantly homogeneously broadened at room temperature, the broadening being the result of the interaction of Cr^{3+} ions with lattice phonons. The width of the transition (FWHM) is $\Delta\nu_0 = 11$ cm$^{-1} = 330$ GHz ($T = 300$°K) and the $2\bar{A}$ and $\bar{E}$ levels have the same lifetime of $\sim 3 \times 10^{-3}$ s ($T = 300$°K). At $T = 77$°K the lifetime increases to 4.3×10^{-3} s, which shows that the room temperature lifetime also has a contribution from nonradiative decay. Note that the lifetime is in the millisecond range and it thus corresponds to an electric-dipole forbidden transition.

Ruby lasers are usually operated in a pulsed regime. For this, a medium-pressure (~500 Torr) xenon flashtube is used, either with the pump configuration as in Fig. 3.2b or, more often, as in Fig. 3.2a. Typical rod diameters range between 5 and 10 mm with a length between 5 and 20 cm. The output performance can be summarized as follows: (i) when Q switched, 10–50 MW in a single giant pulse of 10–20 ns duration, and (ii) when mode locked, a few gigawatts peak power in a pulse of ~10 ps duration. Ruby lasers can also run cw, pumped by a high-pressure mercury lamp.

Ruby lasers, once very popular, are now less widely used, since they have been superseded by their competitors, the Nd:YAG or Nd:glass lasers. Since, in fact, ruby works on a three-level scheme, the required threshold pump energy is about an order of magnitude larger than that for a Nd:YAG laser of comparable size. Ruby lasers are, however, still commonly used for a number of scientific applications, such as pulsed holography and ranging experiments (including military rangefinders).

6.2.2 *Neodymium Lasers*[4-6]

Neodymium lasers are the most popular type of solid state laser. The laser medium is usually either a crystal of $Y_3Al_5O_{12}$ (commonly called YAG, an acronym for *yttrium aluminum garnet*) in which some of the Y^{3+} ions are replaced by Nd^{3+} ions, or simply a glass which has been doped by Nd^{3+} ions. Neodymium lasers can oscillate on several lines, the strongest and thus the most commonly used one being at $\lambda = 1.06$ μm.

A simplified energy-level scheme for Nd:YAG is shown in Fig. 6.2. The energy-level scheme is much the same for Nd:glass since, as already mentioned, the energy levels involved are not strongly influenced by the crystal field. The $\lambda = 1.06$ μm laser transition is the strongest of the ${}^4F_{3/2} \rightarrow {}^4I_{11/2}$ transitions. The two main pump bands occur at 0.73 and 0.8 μm respectively. These bands are coupled by a fast nonradiative decay to

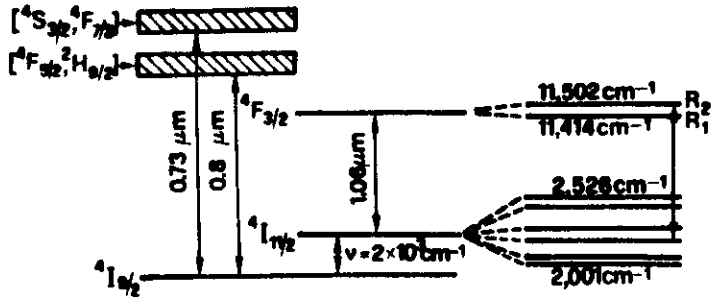

FIG. 6.2. Simplified energy levels of Nd:YAG.

the $^4F_{3/2}$ level, while the lower $^4I_{11/2}$ level is also coupled by a fast nonradiative decay to the $^4I_{9/2}$ ground level. Furthermore, the energy difference between the $^4I_{11/2}$ and $^4I_{9/2}$ levels is almost an order of magnitude larger than kT. Thus it follows that the Nd^{3+} laser works on the four-level scheme. As in the case of ruby, the laser transition is (predominantly) homogeneously broadened and the corresponding width is $\Delta\nu_0 = 6.5\ cm^{-1} = 195$ GHz at $T = 300°K$. The lifetime of the upper laser level is in this case also very long ($\tau = 0.23$ ms) since the transition is forbidden for electric–dipole interaction.

Nd:YAG lasers can operate either cw or pulsed. For both cases, linear lamps in single-ellipse (Fig. 3.2b), close-coupling (Fig. 3.2c), or multiple-ellipse configurations (Fig. 3.3) are commonly used. Medium-pressure (500–1500 Torr) Xe lamps and high-pressure (4–6 atm) Kr lamps are used for the pulsed and cw cases respectively. The rod dimensions are typically the same as those given for ruby. The output performance can be summarized as follows: (i) output power up to 150 W from a single stage and up to 700 W from a cascade of amplifiers, for cw operation; (ii) output power up to 50 MW in Q-switched operation; (iii) pulse duration down to ~20 ps in mode-locked operation. The slope efficiency is about 1–3% for both cw and pulsed operation. Nd:YAG lasers are widely used in a variety of applications such as materials processing (in cw or repetitively pulsed operation), ranging, and laser surgery.

The rod dimensions for Nd:glass may be much larger than those for Nd:YAG (up to perhaps 1 m in length and a few tens of centimeters in diameter). Glass, due to its much lower melting temperature, can in fact be grown much more easily than YAG. Since, however, the thermal conductivity of glass is about an order of magnitude smaller than that of YAG, Nd:glass lasers are usually operated in a pulse regime. The output performance can be summarized as follows: (i) Output energy and peak power in Q-switched operation are comparable with those obtainable from a Nd:YAG rod of comparable dimensions. (ii) Since the laser transition is considerably broader than that of Nd:YAG (the additional, inhomogeneous broadening being due to the variation of ion environments within the glass matrix), pulsewidths as short as ~5 ps can be obtained in mode-locked operation. Nd:glass can be used instead of Nd:YAG in all those applications where the repetition rate of the laser is low enough not to cause thermal problems in the rod. A very important application of Nd:glass is as laser amplifiers in the very high energy systems used in laser fusion experiments. A system based on Nd:glass lasers, delivering pulses with a peak power of more than 20 TW and total energy of ~15 kJ, has already been built (the Shiva laser), and a system which should give an order of magnitude more power and energy is under construction (Nova laser, 200 kJ, 100–300 TW).

6.3 GAS LASERS

In general, for gases, the broadening of the energy levels is rather small (of the order of a few gigahertz or less), since the line-broadening mechanisms are weaker than in solids. For gases at the low pressures often used in lasers (a few Torr), the collision-induced broadening is very small, and the linewidths are therefore essentially determined by Doppler broadening. For this reason optical pumping with lamps of the type used for solid state lasers is not used in the case of gases. This would, in fact, be very inefficient since the emission spectrum of these lamps is more or less continuous, whereas there are no broad absorption bands in the active material. The only case in which laser action has been obtained in a gas by means of optical pumping of this type is that of Cs pumped by a linear lamp containing He. In this case the situation was quite favorable for optical pumping since some He emission lines are coincident with absorption lines of Cs. However, the importance of this laser lies more in its historical significance: Cs, which vaporizes at a temperature of 175°C, is a highly reactive substance.

Gas lasers are usually excited by electrical means, i.e., pumping is achieved by passing a sufficiently large current (dc or pulsed) through the gas. The principal pumping mechanisms occurring in gas lasers have already been discussed in Section 3.3. Other pumping mechanisms which are peculiar to certain lasers (e.g., Penning ionization and charge transfer)

will be introduced in this chapter. We also wish to point out that some gas lasers can also be pumped by mechanisms other than electrical pumping. In particular, we mention pumping by gas-dynamic expansion, chemical pumping, and optical pumping by means of another laser.

Once a given species is in its excited state, it can decay to lower states, including the ground state, by four different processes: (i) collisions between an electron and the excited species, in which the latter gives up its energy to the electron (collision of the second kind), (ii) collisions between atoms (for a gas with more than one constituent), (iii) collisions with the walls of the container, and (iv) spontaneous emission. Regarding this last case, we should always consider the possibility (particularly for the usually very strong UV and VUV transitions) of radiation trapping. This process, already discussed in Section 2.3.4, slows down the effective rate of spontaneous emission.

For a given discharge current, these various processes of excitation and de-excitation lead eventually to some equilibrium distribution of population among the energy levels being established. Thus it can be seen that the production of a population inversion in a gas is a more complicated process than in a solid state laser, owing to the large number of phenomena involved. In general we can say that a population inversion between two given levels will occur when either (or both) of the following circumstances occur: (i) The excitation rate is greater for the upper laser level than for the lower laser level, and (ii) the decay of the upper laser level is slower than that of the lower laser level. We recall that the latter is a necessary condition for cw operation [see (5.26)]. If this condition is not satisfied, however, laser action can still occur under pulsed operation provided condition (i) is fulfilled (self-terminating lasers).

As far as their construction is concerned, many gas lasers have the arrangement illustrated schematically in Fig. 6.3. The gas is contained in a tube of suitable diameter (from a few millimeters to a few centimeters) which is terminated by two end windows inclined at Brewster's angle θ_β. We recall that, for this angle of incidence, a laser beam polarized in the plane of the figure suffers no reflection losses at the window surfaces, and consequently this is the direction of polarization that the laser output

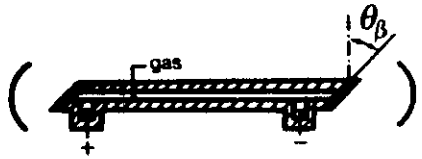

FIG. 6.3. Schematic diagram of a gas laser.

adopts. Spherical mirrors rather than plane mirrors are generally used since the former give better resonator stability (see discussion at the end of Section 4.4.2).

6.3.1 Neutral Atom Lasers

The He–Ne[7–10] laser may be considered to be a typical example (and in fact a particularly important one) of this category of laser. It can oscillate at any of the three following wavelengths: $\lambda_1 = 3.39$ μm, $\lambda_2 = 0.633$ μm, and $\lambda_3 = 1.15$ μm. It was the first gas laser to be made to oscillate (at $\lambda_3 = 1.15$ μm).[7] The 0.633-μm (red) He–Ne laser is one of the most popular and most widely used of lasers.

The energy-level schemes of He and Ne are shown in Fig. 6.4. Laser action occurs between energy levels of Ne, whereas the He is added to assist in the pumping process. In fact, as can be seen from the figure, the levels 2^3S and 2^1S of He are resonant with the levels $2s$ and $3s$, respectively, of Ne. Since the 2^3S and 2^1S levels are metastable, it is found that He proves very efficient in pumping the Ne $2s$ and $3s$ levels by resonant energy transfer. It has been confirmed that this process is the dominant one producing population inversion in the He–Ne laser, although direct electron–Ne collisions also contribute to the pumping. From what has been said earlier, it can be seen that the Ne $2s$ and $3s$ levels can build up their populations, and they are, therefore, likely candidates as upper levels for laser transitions. Taking account of the selection rules, we see that the possible transitions are those to p states. In addition, the decay time of the s states ($\tau_s \simeq 100$ ns) is an order of magnitude longer than the decay time of the p states ($\tau_p \simeq 10$ ns). So, the condition (5.26) for operation as a cw laser is satisfied. From these considerations it is seen that laser oscillation might be expected on any of the transitions a, b, and c of Fig. 6.4. Of the various transitions of type a, the strongest turns out to be that between sublevel $3s_2$ of the $3s$ group and sublevel $3p_4$ of the $3p$ group ($\lambda_1 = 3.39$ μm). Among the transitions of type b, it is the $3s_2 \rightarrow 2p_4$ transition ($\lambda_2 = 0.633$ μm, red) which features in the usual commercial He–Ne laser. The transition $2s_2 \rightarrow 2p_4$ (of type c) produces the wavelength $\lambda_3 = 1.15$ μm. The He–Ne laser will oscillate on transitions a, b, or c according to whether the maximum mirror reflectivity is at λ_1, λ_2, or λ_3. The multilayer dielectric mirrors are, therefore, made in such a way as to give a maximum reflectivity at the desired wavelength.

The laser transition is broadened predominantly by the Doppler effect. For instance, at $\lambda = 632.8$ nm, from (2.106) natural broadening can be

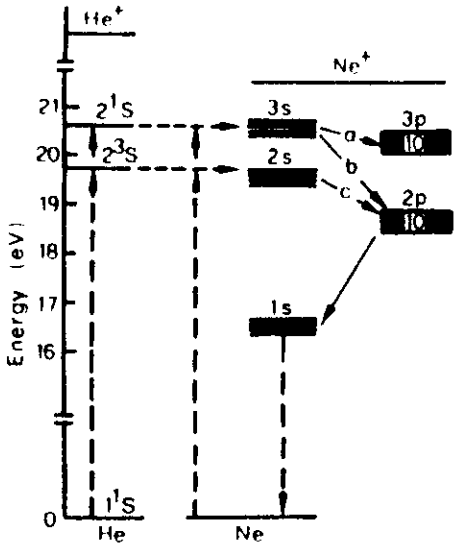

FIG. 6.4. Energy levels of He and Ne.

estimated to be $\Delta\nu_{nat} = 1/2\pi\tau \simeq 19$ MHz, where $\tau^{-1} = \tau_s^{-1} + \tau_p^{-1}$, and τ_s, τ_p are the lifetimes of the s and p states respectively. Collision broadening contributes even less than natural broadening [e.g., for pure Ne, $\Delta\nu_c \simeq 0.6$ MHz at the pressure $p \simeq 0.5$ Torr, see (2.105a)]. Finally it should be noted that the experimentally measured linewidth agrees well with the one calculated above, thus confirming that the effective temperature of the Ne atoms is the ambient temperature.

Early designs of He–Ne laser followed the general scheme of Fig. 6.3, but this has been superseded by an arrangement in which the two ends of the discharge tube are terminated by the two cavity mirrors, whose coated faces are actually in the discharge region. Because of the complicated processes which contribute to the excitation and de-excitation of its levels, the He–Ne laser has optimum values for a number of its operational parameters. In particular, these are (i) optimum value of the product of total gas pressure p and tube diameter D ($pD = 3.6$–4 Torr × mm), (ii) optimum value of the He:Ne ratio ($\sim 5:1$ at $\lambda = 632.7$ nm and $\sim 9:1$ at $\lambda = 1.15$ μm), and (iii) optimum value of the discharge current density J. The fact that there is an optimum value of pD indicates that it is the electron temperature that is being optimized. The elementary theory of a glow discharge in a positive column yields in fact a Maxwellian electron energy distribution whose temperature depends only on the product pD (see Section 3.3.2). The optimum value of current density (at least for the 3.39 and 0.6328 μm transitions) occurs because, at high current densities, de-excitation of the He (2^1S) metastable state occurs not only by diffusion to the walls but also by superelastic collision processes such as

$$\mathrm{He}(2^1S) + e \rightarrow \mathrm{He}(1^1S) + e \tag{6.1}$$

Since the rate of this process is proportional to N_e, the electron density (and hence to J), the overall rate of de-excitation can be written as $k_2 + k_3 J$, where k_2 represents diffusion to the walls and $k_3 J$ represents the superelastic collision process (6.1). Since the excitation rate of the 2^1S level can be expressed as $k_1 J$, the steady state 2^1S population will be given by $Nk_1 J/(k_2 + k_3 J)$, where N is the population of ground-state He atoms. Therefore the 2^1S population of He and hence that of the $3s$ state of Ne will saturate at high current densities, as indicated by the above relation. On the other hand, it has been found experimentally that the population of the lower laser level ($3p$ or $2p$) keeps increasing with J (due to direct pumping from ground-state Ne atoms and to radiative cascading from upper laser levels). As the discharge current density is increased, so the population difference increases to some maximum value and then decreases. Thus the laser gain and hence also the output power will have a maximum value for some particular current density. It should also be noted that the laser gain is found experimentally to vary as D^{-1}, provided pD is kept constant. This can be understood when it is realized that, at constant pD, the electron temperature is constant. Hence, all electron-collision excitation processes scale simply as the number of atoms available for excitation. Since both upper and lower laser levels are ultimately populated by electron-collision processes, their population and hence the laser gain is directly proportional to pressure or to D^{-1} at constant pD.

The preceding considerations indicate that, for a given laser tube, the range of possible current and pressure variation is rather limited. However, by increasing the tube diameter, at constant pD, one can increase the laser output. In this case, the gain decreases approximately as the inverse of the tube diameter, and the cross-sectional area of the discharge increases as the square of the diameter. The combined effect is to produce an output power that is roughly proportional to the tube diameter. Well above threshold, the output power increases linearly with length. A typical optimum output for a 100 cm × 6 mm cylindrical discharge might be 100 mW. Actually, most He–Ne lasers are operated with a bore diameter of 1–6 mm, for reasons of mode control. Since, as we have noted earlier, the linewidth $\Delta\nu$ (for the 633 nm transition) is about 1700 MHz, it is possible to obtain oscillation in a single longitudinal mode by using a cavity length which is short enough to

give a longitudinal mode separation ($c/2L$) comparable to $\Delta\nu$. In fact this implies $L < 15$–20 cm.

He–Ne lasers oscillating on the red transition are widely used for many applications where a low-power visible beam is needed (e.g., alignment, character reading, metrology, holography, video disk memories).

Besides the He–Ne laser there are other neutral atom gas lasers, covering most of the inert gases (He, Ne, Kr, Ar, Xe). In general, for all of these, one finds an energy-level scheme similar to the type shown for Ne in Fig. 6.4, apart from a change in scale. The first excited level ($1s$) is not usually used as a lower laser level since it is metastable. Hence, the levels used in obtaining laser action are higher than the first (or first two) excited levels. Because of this, neutral gas lasers usually operate in the red or near infrared (1–10 μm).

Finally we note that the neutral atom lasers are not represented solely by the inert gases and, in particular, we mention the class of metal vapor lasers (Pb, Cu, Au, Ca, Sr, and Mn). Of these, the most important at present is the Cu laser[10] which oscillates in the green (510.5 nm) where the efficiency is quite high (~1%), and in the yellow, at 578.2 nm. All metal vapor lasers are self-terminating and are therefore operated in a pulsed regime.

A general scheme for the relevant energy levels of this class of lasers is shown in Fig. 6.5. The $g \to 2$ transition is allowed while the $g \to 1$ transition is forbidden by electric-dipole interaction. Under the Born approximation we thus expect the electron-impact cross section of the $g \to 2$ transition to be appreciably larger than that of the $g \to 1$ transition. To accumulate sufficient population in the upper laser level, the $2 \to g$ radiative transition rate, which would usually be fast, must be slowed down to a value comparable to the $2 \to 1$ radiative rate. This means that a sufficient atomic density must be present to produce radiation trapping on the $2 \to g$ transition. Note that since the $1 \to g$ transition is forbidden, the laser can only operate on a pulsed basis with pulse duration of the order of or shorter than the lifetime of level 2. The $1 \to g$ decay usually occurs by collisions with the walls or by atom–atom deactivation. The corresponding decay rate sets an upper limit to the repetition rate of the laser.

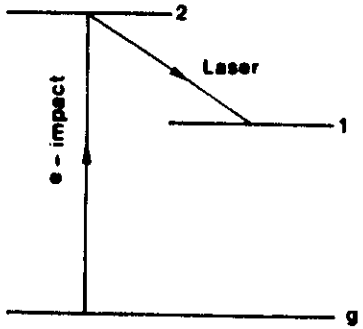

FIG. 6.5. General energy level scheme for a self-terminating metal vapor laser.

The construction of a metal vapor laser follows the general scheme of Fig. 6.3. Two characteristic features are, however, worth noting: (i) Self-terminating lasers exhibit a very high gain per pass. Oscillation can therefore occur even without any mirrors through amplified spontaneous emission (see Section 2.3.4). However, a unidirectional output and a lower threshold are obtained by using a 100% reflecting mirror at one end of the tube and taking the output from the other end. (ii) To obtain the required vapor densities the laser must be operated at high temperature (~1500°C). The laser tube is therefore usually made of alumina and the central region is held in an oven. A few Torr of Ne is also added to the laser tube to prevent deposition of metal vapor on the (cold) end windows. The problem of high operating temperatures can be considerably alleviated by using metal-halogen compounds (e.g., CuBr) rather than the pure metals. In this case the required temperature is considerably lower (~550°C for CuBr) and it can be achieved simply as the result of the heat generated by the discharge (when the laser is operated at sufficiently high repetition rate). However, the vapor then consists of CuBr rather than Cu, and to produce atomic copper, a double discharge technique is used: the first discharge pulse dissociates the CuBr molecule, while the second produces laser action.

Copper vapor lasers have been operated with average powers of ~40 W and repetition rates of ~15 kHz, and in fact provide the most efficient green laser source so far available. They are of interest for underwater communications and remote sensing of submerged objects (seawater is relatively transparent in the blue-green region), and also for some laser-photochemistry applications.

6.3.2 *Ion Lasers*

In the case of an ionized atom, the scale of energy levels is expanded. In this case, in fact, a given electron of the atom experiences the field due to the positive charge Ze of the nucleus (Z being the atomic number of the atom and e the electronic charge) screened by the negative charge $(Z-2)e$ of the remaining electrons. The net effective charge is thus $2e$, whereas, for a neutral atom, it is only e. This expansion in energy scale means that ion lasers typically operate in the visible or ultraviolet regions. We will separate

the ion lasers into two categories: (i) ion gas lasers and (ii) metal vapor lasers.

6.3.2.1 *Ion Gas Lasers*[10-12]

In an ion gas laser, the upper laser level becomes populated by two successive collisions with the electrons in the discharge. The first produces an ion from the neutral atom, while the second excites this ion. The pump process is therefore a two-step process involving the discharge current density J (i.e., it is proportional to J^2 or to higher powers of J, as we shall see later on). For this process to be efficient, a high current density is required. An ion gas laser thus requires a much higher current density than a neutral gas laser.

Of the various ion gas lasers, we will consider in some detail the Ar^+ laser. A level scheme showing the principal energy levels of Ar^+ is given in Fig. 6.6. Population of the upper level ($4p$) of the laser transition can be achieved by three distinct processes: (i) electron collisions with Ar^+ ions in their ground state [process (a)]; (ii) electron collisions with ions in metastable levels [process (b)]; (iii) radiative cascade from higher levels [process (c)]. If we let N_i be the density of Ar^+ ions in the ground state and N_e the electron density, and if we assume that the plasma as a whole is neutral, then we can say that $N_i \simeq N_e$. With this assumption, process (a) produces a pump rate per unit volume $(dN_2/dt)_p$ of the form

$$(dN_2/dt)_p \propto N_e N_i \propto N_e^2 \tag{6.2}$$

Since the discharge reaches a condition in which the electric field is constant, the electron density N_e will be proportional to the discharge current density J. From (6.2) it follows that $(dN_2/dt)_p \propto J^2$. This quadratic dependence on current has been confirmed by observing the variation of spontaneously emitted power as a function of J. This would at first sight appear to be evidence in favor of process (a). However, processes (b) and (c) also give similar dependences of $(dN_2/dt)_p$ on J. This is immediately obvious in the case of process (c). In fact, the populations of those levels from which the cascade process originates will also be proportional to $N_e N_i$ and hence to N_e^2. In the case of process (b) the calculation is slightly more complicated. The population N_m of the metastable levels, which is determined by a balance between excitation and de-excitation processes, is given by

$$N_m \propto N_e N_i/(K + N_e) \tag{6.3}$$

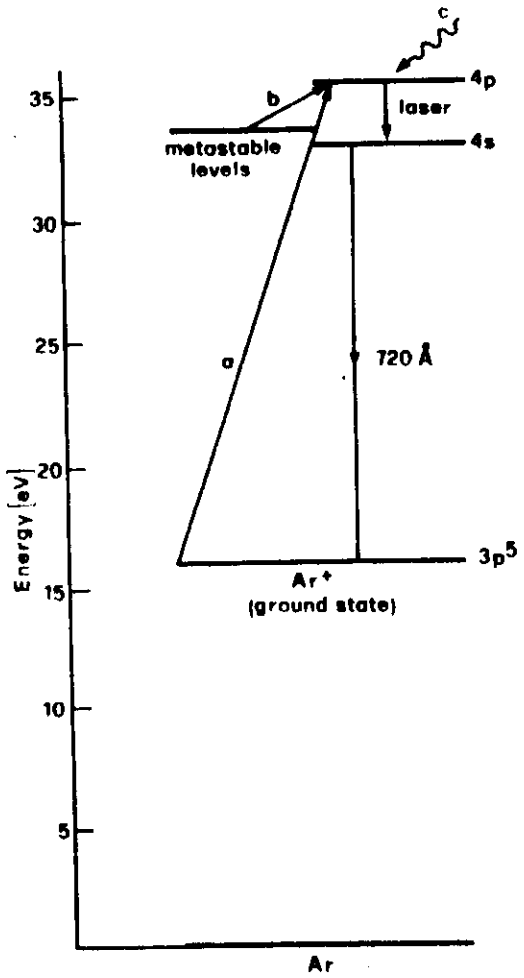

FIG. 6.6. Three different processes contributing to pumping of the upper level ($4p$) of an Ar^+ laser: (a) electron collisions with ground-state ions, (b) electron collisions with metastable-state ions, (c) radiative cascade from higher levels.

The term K in the denominator of (6.3) accounts for spontaneous de-excitation of the metastable level, while the term N_e accounts for de-excitation by electron collisions. From (6.3) one finds that process (b) produces a pumping rate

$$(dN_2/dt)_p \propto N_m N_e \propto N_e^3/(K + N_e) \tag{6.4}$$

However, since the metastables are more likely to be de-excited by electron collisions than by spontaneous emission (i.e., $K \ll N_e$), it is seen from (6.4) that one again has the result that $(dN_2/dt)_p \propto N_e^2$. It is probable then that all three of the processes listed contribute to populating the laser level. It has been demonstrated, in fact, that a fraction, 23–50%, of the upper level population is due to the cascade process (c). Finally, we note that the lifetime of the upper laser level is $\sim 10^{-8}$ s, while the lower laser level ($4s$) is connected to the ground state by a radiative transition with a much shorter lifetime (10^{-9} s). So in this case also, condition (5.26) is satisfied. The Doppler linewidth $\Delta\nu_0^*$ is ~3500 MHz and from (2.113) it is seen that this implies a temperature $T \simeq 3000°$K. The ions are therefore very "hot" as a result of being accelerated by the electric field in the discharge.

A schematic diagram of an Ar^+ laser tube construction is given in Fig. 6.7. Because of the high current density there is a migration of Ar^+ ions towards the cathode (cataphoresis), and a return tube, as shown in the figure, is provided to compensate for this. Obviously, the return tube length must be greater than that of the laser tube to prevent the discharge passing along the return tube instead of the laser tube. At the high current densities involved, one of the most serious technological problems is damage to the tube caused by ions colliding with it ($T \simeq 3000°$K). Because of this, the tube is usually made of a ceramic material (beryllia) or of graphite. Also, a static magnetic field is applied, parallel to the tube axis, in the discharge region. With this arrangement the Lorentz force reduces the rate of diffusion of electrons towards the walls. This increases the number of free electrons at the center of the tube which leads to an increase in the pump rate and hence in the output power. By confining the discharge towards the center of the tube, the magnetic field also alleviates the problem of wall damage. Unlike the He–Ne laser, in this case, the gain does not depend on the internal diameter of the tube since an accumulation of population in the metastable levels does not decrease the population inversion. In commercial lasers, however, the tube diameter is kept small (a few millimeters) to confine oscillation to the TEM_{00} mode and to reduce the total current

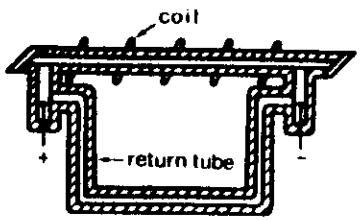

FIG. 6.7. Schematic diagram of an Ar^+ laser tube

required. On the other hand, if one wants to increase the output power or reduce the problem of wall damage, there is an advantage to be gained from using substantially greater diameters.

The Ar^+ laser can oscillate at a number of wavelengths, the most intense being at $\lambda_1 = 488$ nm (blue) and $\lambda_2 = 514.5$ nm (green). It is possible to achieve oscillation on just a single line using the scheme of Fig. 5.7. An important characteristic of the Ar^+ laser (and of ion lasers in general) is that the output power increases rapidly with increasing discharge current. Unlike the He–Ne laser, the output power of the Ar^+ laser continues to increase with increasing excitation power. This is because the process of saturation of inversion (in this case due to resonance trapping of radiation on the 720 Å transition of Fig. 6.6) only becomes significant for current densities much higher than those that can be reached in practice. For the reasons given above, it has been possible to obtain very high output powers from Ar^+ lasers (up to 200 W continuous from a 1-cm-diameter tube). The laser efficiency is very low, however ($< 10^{-1}$). Argon lasers are widely used as a pump for cw dye lasers, for a variety of scientific applications (light–matter interactions), in laser printers, in laser surgery, and in the field of laser entertainment.

We conclude this section by mentioning the Kr^+ laser which, of the various other ion gas lasers, is the most widely used. It also oscillates at a number of wavelengths, of which the most powerful is in the red (647.1 nm).

6.3.2.2 Metal Vapor Lasers

The following metals have been used in vapor form to produce laser action: Sn, Pb, Zn, Cd, and Se. Of these lasers, the most widely used are those using Cd or Se vapors. Cd vapor produces strong cw laser action at the wavelengths $\lambda_1 = 441$ nm and $\lambda_2 = 325$ nm. The latter wavelength is particularly interesting for many applications since it falls in the UV region of the e.m. spectrum. Se vapor gives strong cw laser action on at least 19 wavelengths that cover most of the visible spectrum. Unlike ion gas lasers, in metal vapor lasers there are two quite different pump processes[†] that can be used: (i) Penning ionization, (ii) charge transfer ionization. Since these are single-step processes, the corresponding pump rate is now proportional to J rather than to J^2 (or J^3) as for the ion gas lasers. Much lower current

[†]The Ar^+ laser cannot use these processes because its laser levels are very high in energy (~35 eV, see Fig. 6.6).

density and electrical power per unit length are therefore required for metal vapor lasers compared to ion gas lasers.

The Penning ionization process can be written as

$$A^* + B \rightarrow A + B^+ + e \tag{6.5}$$

where the ion B^+ in its final state may or may not be internally excited. Of course, this can only occur if the excitation energy of the excited atom A^* is greater than or equal to the energy required to ionize the other atom B. The surplus energy is transformed to kinetic energy of the electron. The process is most prominent when the excited species A^* is in a metastable state. Note that, unlike resonant energy transfer, Penning ionization is a nonresonant process: The excitation energy of A^* need only be greater than the ionization energy plus the excitation energy of atom B (if atom B is to be left in an excited state). Any surplus energy can in fact be removed as kinetic energy of the ejected electron. Charge transfer ionization, on the other hand, is a process of the type

$$A^+ + B \rightarrow A + (B^+)^* \tag{6.6}$$

Here the ionization energy of atom A is transformed into ionization plus excitation energy of atom B. Since no electrons are ejected in this case, the process must be resonant: The ionization energy of A must equal the ionization plus excitation energy of B. The process is particularly effective if the A^+ ion is metastable (i.e., if it has a long lifetime).

After this brief discussion of the main pump mechanisms of metal vapor lasers, we will now describe the two most widely used lasers in this category: the He–Cd and He–Se lasers. The energy levels of the He–Cd system are shown in Fig. 6.8. The Cd laser is thus seen to be pumped predominantly by the Penning ionization process. The 2^1S and 2^3S metastable states of He can excite either the $^2D_{3/2}$ and $^2D_{5/2}$ states or the $^2P_{3/2}$ and $^2P_{1/2}$ states of Cd^+. Although the process is not resonant, it has been found that the cross section for excitation of the D states is about three times greater than that of the P states. What is more important, however, is that the lifetime of D states (10^{-7} s) is much longer than the lifetime of P states (10^{-9} s). Population inversion between the D and P states can, therefore, be produced readily and laser action has been achieved on the $^2D_{3/2} \rightarrow {}^2P_{1/2}$ ($\lambda = 325$ nm) and the $^2D_{5/2} \rightarrow {}^2P_{3/2}$ ($\lambda = 441.6$ nm) lines. The Cd^+ ions then drop to the $^2S_{1/2}$ ground state by radiative decay. In the case of the He–Se laser, the energy of the upper laser levels of the Se^+ ion (i.e., the sum of the ionization plus excitation energy of the Se atom) is ~25 eV (Fig. 6.9), i.e., greater than the excitation energy of the He metastable

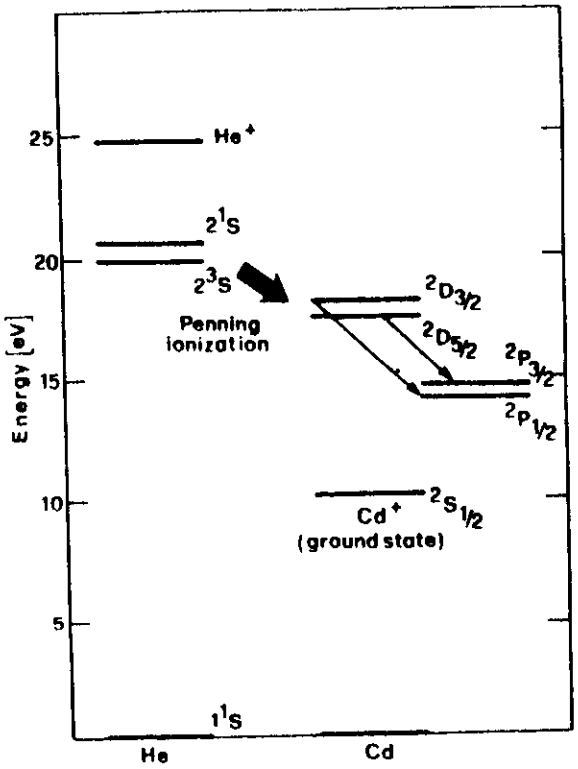

FIG. 6.8. Relevant energy levels of the He–Cd laser.

states. Therefore the upper laser levels can only be pumped by charge transfer ionization (the He^+ ion has in fact an energy of ~25 eV). This process is very effective since the He^+ ion has a long lifetime (it is determined only by electron recombination).

In its construction, a metal vapor laser is not very different from that shown in Fig. 6.3. In one possible configuration, however, the tube has a small reservoir near the anode to contain the metal. This reservoir is heated to a high enough temperature (~250°C) to produce the desired vapor pressure in the tube. When the vapor reaches the discharge, some of the atoms are ionized and these migrate toward the cathode. The discharge produces enough heat to prevent condensation of the vapor on the walls of the tube. The vapor condenses, however, when it reaches the cathode region, where there is no discharge, and the temperature is low. The net

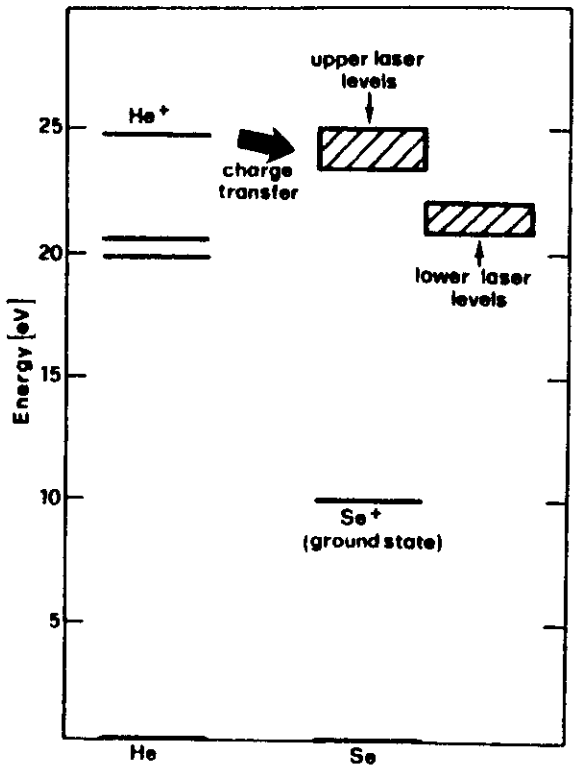

FIG. 6.9. Relevant energy levels of the He–Se laser.

result is a continuous flow of metal vapor from the anode to the cathode (this flow is called *cataphoresis*). Therefore a sufficient supply of Cd (1 g per 1000 h) must be provided for the life of the tube. He–Cd and He–Se lasers can give output powers of 50–100 mW, which places them in an intermediate position between red He–Ne lasers (a few milliwatts) and Ar^+ lasers (a few watts). He–Cd lasers are attractive for many applications where a blue or UV beam of moderate power is of interest (e.g., facsimile systems, reprographic systems, and Raman and fluorescence experiments).

6.3.3 *Molecular Gas Lasers*

These lasers exploit transitions between the energy levels of a molecule. Depending on the type of transition involved, molecular gas lasers can be

placed in one of the three following categories: (i) Vibrational–rotational lasers. These lasers use transitions between vibrational levels of the same electronic state (the ground state). The energy difference between the levels involved in this type of transition (see Section 2.9.1) means that these lasers oscillate in the middle- and far-infrared (5–300 μm). (ii) Vibronic lasers. These lasers use transitions between vibrational levels of different electronic states (the word "vibronic" is a contraction from the words "vibrational" and "electronic"). In this case the oscillation wavelength falls in the visible/UV region. (iii) Pure rotational lasers which use transitions between different rotational levels of the same vibrational state. The corresponding wavelength falls in the far infrared (25 μm to 1 mm). Laser action is more difficult to achieve in this type of laser since the relaxation between rotational levels is generally very fast. These lasers are usually pumped optically,[13] using the output of another laser as the pump (commonly a CO_2 laser). Optical pumping excites the given molecule (e.g., CH_3F, $\lambda = 496$ μm) to a rotational level belonging to some vibrational state above the ground level. Laser action then takes place between rotational levels of this upper vibrational state.

6.3.3.1 *Vibrational–Rotational Lasers*

Of the various vibrational–rotational lasers, we will discuss the CO_2 laser in some detail.[14,15] This laser uses a mixture of CO_2, N_2, and He. Oscillation takes place between two vibrational levels in CO_2, while, as we shall see, the N_2 and He greatly improve the efficiency of laser action. The CO_2 laser is actually one of the most powerful lasers (output powers of ~80 kW have been demonstrated from a CO_2 gas-dynamic laser) and one of the most efficient (15–20%). Only the CO laser and the pulsed, electron-beam-initiated HF chemical laser have been reported with higher efficiencies.

Figure 6.10 shows the vibrational energy-level schemes for the electronic ground states of the CO_2 and N_2 molecules. N_2, being a diatomic molecule, has only one vibrational mode, and the lowest two vibrational levels ($v = 0$, $v = 1$) are indicated in the figure. The energy levels for CO_2 are more complicated since CO_2 is a linear triatomic molecule. In this case, there are three nondegenerate modes of vibration (Fig. 6.11): (1) symmetric stretching mode, (2) bending mode, and (3) asymmetric stretching mode. The oscillation behavior is therefore described by means of three quantum numbers n_1, n_2, and n_3, which give the number of quanta in each vibrational mode. The corresponding level is therefore designated by these three

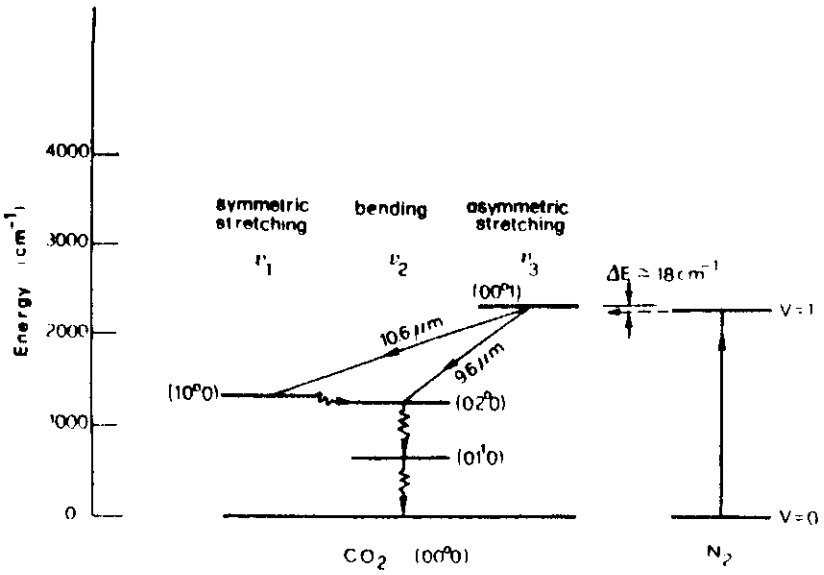

FIG. 6.10. The lowest vibrational levels of the ground electronic state of an N_2 molecule and a CO_2 molecule (for simplicity, the rotational levels are not shown).

quantum numbers written in the order n_1, n_2, n_3. For example, the 01^10 level[†] corresponds to an oscillation in which there is one vibrational quantum in mode 2. Since mode 2 has the smallest force constant of the three modes (the vibrational motion is transverse), it follows that this level will have the lowest energy. Laser action takes place between the 00^01 and 10^00 levels ($\lambda \simeq 10.6$ μm) although it is also possible to obtain oscillation between 00^01 and 02^00 ($\lambda \simeq 9.6$ μm). In fact, taking account of the rotational levels (which are not shown in Fig. 6.10), oscillation can take place on two sets of lines centered around $\lambda = 10.6$ μm and $\lambda = 9.6$ μm, respectively. The 00^01 level is very efficiently pumped by two processes:

(i) Electron Collisions. $e + CO_2(00^00) \rightarrow e + CO_2(00^01)$. The electron

[†] The superscript (which we will denote by l) on the bending quantum number arises from the fact that the bending vibration is, in this case, doubly degenerate: it can occur both in the plane of Fig. 6.11 and in the plane orthogonal to it. A bending vibration therefore consists of a suitable combination of these two vibrations. The superscript l characterizes this combination; more precisely, $l\hbar$ gives the angular momentum of this vibration about the axis of the CO_2 molecule. For example, in the 02^00 state ($l = 0$) the two degenerate vibrations combine in such a way to give an angular momentum $l\hbar = 0$.

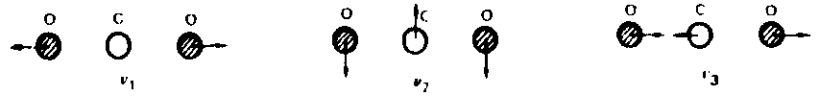

FIG. 6.11. The three fundamental modes of vibration for a CO_2 molecule: (ν_1) symmetric stretching mode, (ν_2) bending mode, (ν_3) asymmetric stretching mode.

collision cross section for this process is very large. Electron collisions populate the 00^01 level preferentially (and not the lower laser levels 10^00 and 02^00), probably because the $00^01 \rightarrow 00^00$ transition is an allowed optical transition, whereas the $00^00 \rightarrow 10^00$ transition is not.

(ii) Resonant Energy Transfer from N_2 Molecule. This process is also very efficient because of the small energy difference between the two levels ($\Delta E = 18$ cm^{-1}). In addition the excitation of N_2 from the ground level to the $v = 1$ level by electron collisions is a very efficient process and the $v = 1$ level is metastable (the $1 \rightarrow 0$ transition is forbidden for electric-dipole radiation since, by virtue of its symmetry, a N–N molecule cannot have a net electric dipole moment). Finally the higher vibrational levels of N_2 are also closely resonant ($\Delta E < kT$) with the corresponding CO_2 levels (up to 00^04), and transitions between the excited levels $00n$ and the 001 are fast. In fact they occur very effectively through collisions with ground-state CO_2 molecules in the following (nearly) resonant process:

$$CO_2(0,0,n) + CO_2(0,0,0) \rightarrow CO_2(0,0,n-1) + CO_2(0,0,1) \qquad (6.7)$$

This process tends to degrade all excited molecules to the (0, 0, 1) state. Actually, level thermalization between the (0, 0, 1) and the upper vibrational state is readily established in this way, and this vibrational system can be described by a vibrational temperature T_1. It can be seen then that, through these various processes, pumping of the upper laser level is a very efficient process, and this explains the high efficiency of the CO_2 laser.

The next point to consider is the decay of the upper laser level and how it compares with the decay rate of the lower laser level. Although the transitions $00^01 \rightarrow 10^00$, $00^01 \rightarrow 02^00$, $10^00 \rightarrow 01^10$, and $02^00 \rightarrow 01^10$ are optically allowed, the corresponding decay times τ_{sp} for spontaneous emission are very long (we recall that $\tau_{sp} \propto 1/\omega^3$). The decay of these various levels is therefore essentially determined by collisions. Accordingly, the decay time τ_s of the upper laser level can be obtained from a formula of the type

$$\frac{1}{\tau_s} = \sum a_i p_i \qquad (6.8)$$

where the p_i are partial pressures and the a_i are constants which are characteristic of the gases in the discharge. Taking, for example, the case of

a partial pressure of 1.5 Torr for CO_2, 1.5 Torr for N_2, and 12 Torr for He, one finds that the upper level has a lifetime $\tau_s \simeq 0.4$ ms. As far as the relaxation rate of the lower level is concerned, we begin by noting that the $100 \rightarrow 020$ transition is very fast and it occurs even in an isolated molecule. In fact the energy difference between the two levels is much smaller than kT. Furthermore, a coupling between the two states is present (Fermi resonance) because a bending vibration tends to induce a change of distance between the two oxygen atom (i.e., induce a symmetric stretching). Levels 10^00 and 02^00 are then effectively coupled to the 01^10 level by a near-resonant, collision process involving CO_2 molecules in the ground state:

$$CO_2(10^00) + CO_2(00^00) \rightarrow CO_2(01^10) + CO_2(01^10) + \Delta E \quad (6.9a)$$

$$CO_2(02^00) + CO_2(00^00) \rightarrow CO_2(01^10) + CO_2(01^10) + \Delta E' \quad (6.9b)$$

The two above processes have a very high probability since ΔE and $\Delta E'$ are much smaller than kT[†]. It follows, therefore, that the three levels 10^00, 02^00, and 01^10 reach thermal equilibrium in a very short time. This amounts to saying that the populations of these three levels can be described by a vibrational temperature T_2. Generally this temperature T_2 is not the same as T_1. We are therefore left with the decay from the 01^10 to the ground level 00^00. If this decay were slow, it would lead to an accumulation of molecules in the 01^10 level during laser action. This in turn would produce an accumulation in the 10^00 and 02^00 levels since these are in thermal equilibrium with the 01^10 level. Thus a slowing down of the decay process of all three levels would occur, i.e., the $01^10 \rightarrow 00^00$ transition would constitute a "bottleneck" in the overall decay process. It is, therefore, important to look into the question of the lifetime of the 01^10 level. This lifetime is also given by an expression of the type (6.8), and in this case the lifetime is greatly influenced by the presence of He (i.e., the coefficient a_i for He is very large). For the same partial pressures as considered in the example above, one obtains a lifetime of about 20 μs. It follows from the above discussion that this will also be the value of the lifetime of the lower laser level. Therefore condition (5.26) is easily satisfied in this case. Note that, since the $01^10 \rightarrow 00^00$ transition is the least energetic transition in any of the molecules in the discharge, relaxation from the 01^10 level can only occur by transferring this vibrational energy to translational energy of the colliding partners (V–T relaxation). Finally, we note that the presence of

[†] Relaxation processes in which vibrational energy is given up as vibrational energy of another like or unlike molecule are usually referred to as V–V relaxations.

He has another valuable effect. The He, because of its high thermal conductivity, helps to keep the CO_2 cool by conducting heat away to the walls. A low translational temperature for CO_2 is necessary to avoid population of the lower laser level by thermal excitation. The energy separation between the levels is, in fact, comparable to kT. In conclusion, the beneficial effects of the N_2 and He can be summarized as follows: The N_2 helps to produce a large population in the upper laser level while the He helps to empty population from the lower laser level.

From the point of view of their construction, CO_2 lasers can be separated into six categories: (i) lasers with longitudinal flow, (ii) sealed-off lasers, (iii) waveguide lasers, (iv) transverse-flow lasers, (v) transversely excited atmospheric pressure (TEA) lasers, and (vi) gas-dynamic lasers.

(i) Lasers with Longitudinal Gas Flow. The first CO_2 laser operation[16] was achieved in a laser of this type, and Fig. 6.12 shows one possible configuration. The mirrors can be internal (in contact with the gas), as in the figure, or external. In the latter case, the tube has a Brewster-angle window at each end (see Fig. 6.3). In the former case, at least one of the (metallic) mirrors needs to be kept at high voltage. The main reason for flowing the gas mixture is to remove the dissociation products, in particular CO, which would otherwise contaminate the laser. It is important to note that, except for very high flow velocities (supersonic flows), the heat dissipated in the discharge is removed by heat diffusion to the walls of the tube (which is water-cooled). In this case there is a maximum laser output power that can be obtained per unit length of the discharge (50–60 W/m) independent of the tube diameter. This comes about as a result of the

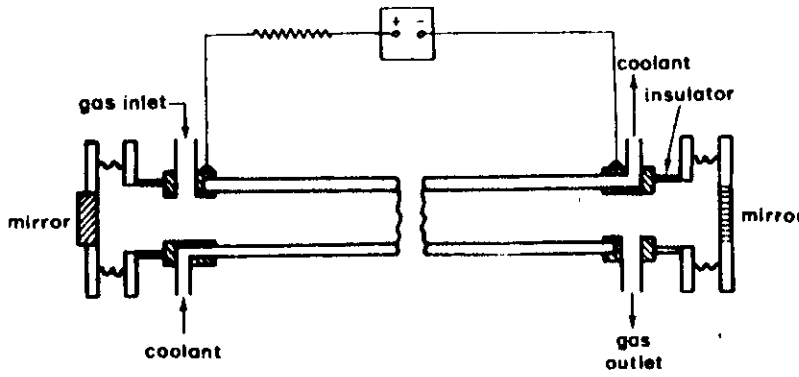

FIG. 6.12. Schematic diagram of a CO_2 laser with longitudinal gas flow.

following three circumstances: (1) If the tube diameter and the pressure are fixed, there will be some optimum value of current density. This is due to the fact that, at high current densities, there will be a rise in gas temperature with a consequent increase in population of the lower laser level. (2) If the diameter is fixed, there will be some optimum set of values for the partial pressures of the gases in the mixture and particularly of the CO_2. To explain this optimum CO_2 pressure, we begin by noting that from equations (5.17) and (5.18) one has the result that, at threshold, the number of atoms pumped per second into the upper laser level is

$$(dN_2/dt)_p = W_p(N_t - N_c) = (\gamma/\sigma l\tau) \propto \Delta\omega_0/\tau$$

where $\Delta\omega_0$ is the linewidth and τ is the lifetime of the upper level. Since this lifetime is determined by collisions, it is inversely proportional to the pressure p. The transition linewidth is the combined result of Doppler broadening and collision broadening. Therefore, $\Delta\omega_0$ increases with increasing pressure (for high pressures $\Delta\omega_0 \propto p$). Since the threshold electrical power P_e is proportional to $(dN_2/dt)_p$, it follows that P_e will increase with increasing pressure ($P_e \propto p^2$ at high pressures). The power dissipated in the gas therefore increases rapidly with increasing pressure. Above a certain pressure this will produce such a large temperature rise that the output power decreases. (3) The optimum values for current density J and pressure p are more or less inversely proportional to the laser tube diameter D (e.g., $p_{op} = 15$ Torr for $D = 1.5$ cm). This can be understood when one realizes that for larger diameters the generated heat has more difficulty in escaping to the walls. If we call σ_e the CO_2 cross section for electron impact excitation to the 00^01 level, the number of molecules pumped into the upper level per second is given by (3.19):

$$\left(\frac{dN_2}{dt}\right)_p = \frac{J\sigma_e(N_t - N_c)}{e} \simeq \frac{J\sigma_e N_t}{e}$$

where e is the electron charge. For pump rates well above threshold, the output power is proportional to $(dN_2/dt)_p$ and therefore

$$P \propto JN_tV_a \propto JpD^2l \tag{6.10}$$

where V_a is the volume of active material and l its length. Since the optimum values of J and p are inversely proportional to D, it follows that the optimum value of P depends only on the length l.

The total gas pressure in a longitudinal-flow CO_2 laser is of the order of 15 Torr (for $D = 1.5$ cm). At this pressure a major contribution to the laser linewidth comes from Doppler broadening (~50 MHz). The small value of Doppler linewidth (compared to visible gas lasers) is a result of the low frequency ω_0 of the transition. The small Doppler width also means that in this case collision broadening is not negligible. In fact it amounts to $\Delta\nu_c = 7.58(\psi_{CO_2} + 0.73\psi_{N_2} + 0.6\psi_{He})p(300/T)^{1/2}$ MHz, where the ψ are fractional partial pressures of the gas mixture and p the total pressure (in Torr). With this small linewidth, longitudinal-flow lasers automatically have their oscillation confined to a single longitudinal mode provided the resonator length is less than ~1 m. In this case, therefore, it becomes necessary to finely adjust the cavity length to ensure that a mode falls at the center of the gain curve. Actually, in our discussion so far we have ignored the fact that the upper laser level is made up from many rotational levels whose population is given by the Boltzmann distribution (see Fig. 6.13).† Accordingly, the laser transition consists of several equally spaced rotational-vibrational transitions (separated by ~2 cm^{-1}) belonging to both P and R branches (see Fig. 2.25). However, it is usually only the rotational transition with the largest gain, i.e., originating from the most heavily populated level, that actually oscillates [$P(22)$ transition]. This is because the rate of thermalization of the rotational levels (~10^7 s^{-1} $Torr^{-1}$) is faster than the rate of decrease of population (due to spontaneous and stimulated emission) of the rotational level which is oscillating. Therefore, the entire

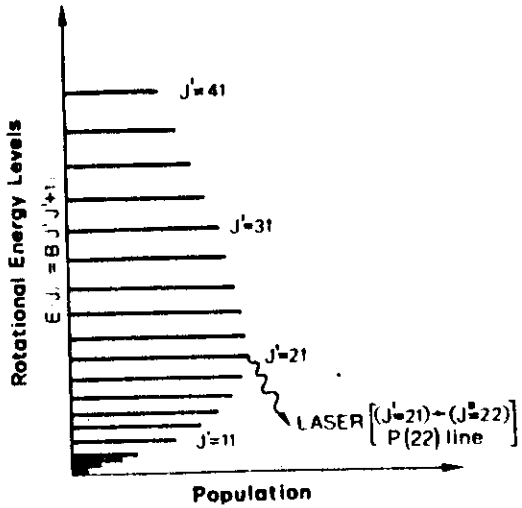

FIG. 6.13. Relative population of the rotational levels of a given vibrational level (e.g., the upper laser level of CO_2).

†Note that, for symmetry reasons, only levels with odd values of J are occupied.

population of rotational levels will contribute to laser action on the rotational level with highest gain. It was mentioned earlier that laser action can take place either on the $00^0 1 \rightarrow 10^0 0$ transition or on the $00^0 1 \rightarrow 02^0 0$ transition. Since the first of these has the greater gain and since both transitions have the same upper level, it follows that it is usually the $00^0 1 \rightarrow 10^0 0$ transition (10.6 μm) which oscillates. To summarize, we can say that oscillation usually takes place in a single rotational line of the $00^0 1 \rightarrow 10^0 0$ transition. To obtain oscillation on the 9.6-μm line or on a different rotational line, some appropriate frequency-selective device is placed in the cavity to suppress laser action on the line with highest gain. In fact the arrangement of Fig. 5.7b is commonly used. Finally we note that, with its long lifetime for the upper laser level ($\tau \simeq 0.4$ msec), the CO_2 laser lends itself particularly well to Q-switched operation. Repetitive Q switching is achieved by spinning one of the two mirrors at high speed while the gas is pumped by a continuous electrical discharge. However, the average power obtained in this way is only a small fraction (~5%) of that available from the same laser when operated cw. This is due to the fact that, when Q switched, the output pulse duration is comparable to the time taken for thermalization of the rotational levels. It is then no longer possible for the entire population of the rotational levels to contribute to laser action on the rotational line which is oscillating.

CO_2 lasers with longitudinal gas flow typically produce output powers of 50–500 W. Powers of 50–100 W are needed for laser surgery while powers up to 500 W are used in applications such as ceramic scribing, cutting of nonmetallic materials, resistor trimming, and welding of metals with a few millimeters thickness.

(ii) Sealed-off Lasers. If the flow of the gas mixture were stopped in the arrangement shown in Fig. 6.12, laser action would cease in a few minutes. This is because the chemical reaction products formed in the discharge (CO, in particular) would no longer be removed and would instead be absorbed in the walls of the tube or react with the electrodes, thus upsetting the CO_2–CO–O_2 equilibrium. Ultimately this would lead to dissociation of the CO_2. For a sealed-off laser, some kind of catalyst must be present in the gas tube to promote the regeneration of CO_2 from the CO. A simple way to achieve this is to add a small amount of H_2O (1%) to the gas mixture. This leads to regeneration of CO_2, probably through the reaction

$$CO^* + OH \rightarrow CO_2^* + H \qquad (6.11)$$

involving vibrationally excited CO and CO_2 molecules. The relatively small amount of H_2O vapor required may be added in the form of hydrogen and oxygen gas. In fact, since oxygen is produced during the dissociation of CO_2, it is found that only hydrogen need be added. Another way of inducing the recombination reaction relies on the use of a hot (300°C) Ni cathode which acts as a catalyst. With these techniques, lifetimes for sealed-off tubes in excess of 10,000 h have been demonstrated.

Sealed-off lasers have produced output powers per unit length of ~60 W/m, comparable to those for longitudinal-flow lasers. Low power (~1 W) sealed-off lasers of short length and hence operating in a single mode are often used as local oscillators in optical heterodyne experiments. Sealed-off CO_2 lasers of somewhat higher power (~10 W) are attractive for laser microsurgery.

(iii) Waveguide Lasers.[17] If the diameter of the laser tube in Fig. 6.12 is reduced to about 1 mm, a situation is reached where the laser radiation is guided by the inner walls of the tube. Such waveguide CO_2 lasers have a low diffraction loss. Tubes of BeO or SiO_2 have been found to give the best performance. The power per unit length and efficiency of a waveguide laser are both somewhat smaller than the corresponding values for a conventional longitudinal-flow laser. The main advantage of a waveguide laser is the relatively large tuning range (~1 GHz) resulting from the increased optimum operating pressure (100–200 Torr). This is a very attractive feature where the laser is to be used as a local oscillator in an optical heterodyne experiment.

(iv) Transverse-Flow Lasers. We have seen that, for longitudinal-flow lasers (and also for sealed-off lasers) there is some maximum laser power that can be extracted. This is essentially due to a heating problem; with an efficiency of 20%, about 80% of the electrical power is dissipated in the discharge as heat. In those lasers the heat removal is effected simply by diffusion from the center of the tube towards the walls (which are cooled). A much more efficient way is to flow the gas perpendicular to the discharge (Fig. 6.14). If the flow is fast enough, the heat gets carried away by convection rather than by diffusion. The saturation of output power versus discharge current density now occurs at much higher values than in the longitudinal-flow arrangement. The optimum total pressure is now an order of magnitude greater (~100 Torr) and consequently, output powers well in excess of 1 kW can be obtained from these lasers with a length of ~1 m (see also Fig. 5.13). The increased total pressure p requires a corresponding increase of the electric field $\mathscr{E}$ in the discharge. In fact, for optimum operating conditions, the ratio $\mathscr{E}/p$ must remain approximately the same for all of these cases since this ratio determines the average energy of the

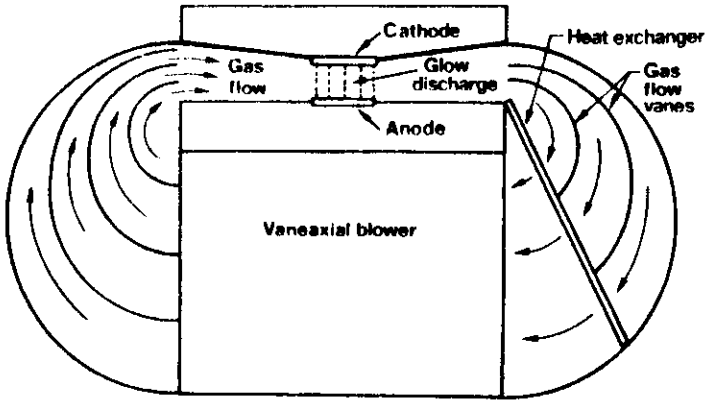

FIG. 6.14. Schematic diagram for a transverse-flow CO_2 laser.

discharge electrons [see (3.23)]. With this larger value of electric field, a longitudinal-discharge arrangement such as in Fig. 6.12 would be impractical since it would require a very high applied voltage (100–500 kV for a 1-m discharge). For this reason, the discharge is usually applied in a direction perpendicular to the resonator axis (lasers with transverse electric field, TE lasers). TE discharges can be classified into two types: self-sustained and non-self-sustained. In the self-sustained discharge the gas ionization is effected by the discharge. Therefore the value of $\mathscr{E}/p$ must be sufficiently large to promote avalanche ionization of the gas. In the non-self-sustained discharge, ionization is provided by auxiliary means such as a source of ionizing radiation. The $\mathscr{E}/p$ ratio can then be reduced to the value which maximizes the excitation of the upper laser level. In Fig. 6.15 an example is shown in which the main discharge is sustained by an auxiliary electron beam.

TE CO_2 lasers with fast transverse flow and high output powers (1–15 kW) are used in a great variety of metalworking applications (cutting, welding, surface hardening, surface metal alloying).

(v) Transversely Excited Atmospheric Pressure CO_2 Lasers.[18] In a cw TE CO_2 laser, it is not easy to increase the operating pressure above ~ 100 Torr. Above this pressure and at the current densities normally used, glow discharge instabilities set in and result in the formation of arcs within the discharge volume. To overcome this difficulty, the voltage can be applied to the transverse electrodes in the form of a pulse. If the pulse duration is sufficiently short (a fraction of a microsecond), the discharge instabilities

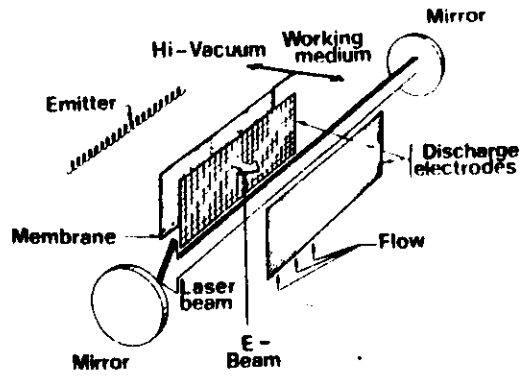

FIG. 6.15. *E*-beam sustained TE CO_2 laser [after Daugherty[37]].

have no time to develop and the operating pressure can then be increased up to and above atmospheric pressure. These lasers are therefore referred to as TEA lasers, the abbreviation standing for transversely excited atmospheric pressure. These lasers thus produce a pulsed output and are capable of large output energies per unit volume of the discharge (10–50 J/liter). To avoid arc formation, some form of ionization is also applied, which just precedes the voltage pulse producing the gas excitation (*pre-ionization*). A possible configuration is shown in Fig. 6.16, where the cathode structure consists of a trigger electrode in close proximity to a mesh and insulated from it by a dielectric sheet. A trigger pulse of high voltage is first applied between the trigger electrode and the mesh, and ions will thus be created near the cathode (corona effect). The main discharge pulse is then applied between the anode and the mesh cathode to excite the entire laser volume. This excitation method is often referred to as the double-discharge technique. Other preionization techniques include the use of pulsed *e*-beam guns (*e-beam pre-ionization*) or of suitable UV-emitting sparks to produce UV photoionization (*UV pre-ionization*). Since the transverse dimensions of

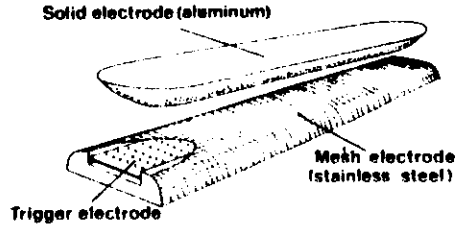

FIG. 6.16. Electrode assembly for double-discharge TEA CO_2 laser [after Richardson *et al.*[39]].

the laser are usually large, the two end mirrors are often chosen to give an unstable resonator configuration (positive-branch unstable confocal resonator, see Fig. 4.26). For low pulse repetition rates (~1 Hz), it proves unnecessary to flow the gas mixture. For higher repetition rates (up to a few kilohertz) the gas mixture is flowed transversely to the resonator axis and is cooled by a suitable heat exchanger. Another interesting characteristic of these lasers is their relatively broad linewidths (~4 GHz at $p = 1$ atm, due to collision broadening). Thus, by mode-locking TEA lasers, optical pulses with less than 1-ns duration have been produced. A very important application of TEA CO_2 lasers is in laser fusion experiments. A system based on TEA CO_2 lasers, delivering pulses with a peak power of 20 TW and total energy of 10 kJ, has already been built (the Helios laser). A system which should give an order of magnitude more power and energy is under construction (Antares laser, 100 kJ, 100–200 TW).

(vi) Gas-Dynamic CO_2 Laser.[19] The gas-dynamic CO_2 laser deserves a special mention since, in this laser, population inversion is not produced by an electrical discharge but by rapid expansion of a gas mixture (containing CO_2) which has initially been heated to a high temperature. Population inversion is produced downstream in the expansion region. Gas-dynamic CO_2 lasers have produced some of the largest powers so far reported in the unclassified literature.

The operating principle of a gas-dynamic laser can be summarized as follows (see Fig. 6.17). Suppose that the gas mixture is first held at high temperature (e.g., $T = 1400°K$) and pressure (e.g., $p = 17$ atm) in an appropriate container. Since the gas is initially in thermal equilibrium and at a high temperature, the population of the 00^01 level of CO_2 will be appreciable (~10% of the ground-state population, see Fig. 6.17b). The lower-level population is, of course, higher than this (~25%), and there is no population inversion. Now suppose the mixture is made to expand through some expansion nozzles (Fig. 6.17c). Since the expansion is adiabatic, the translational temperature of the mixture will be reduced to a much lower value. Due to V–T relaxation, the populations of both upper and lower laser levels will tend to relax to the new equilibrium values. However, since the lifetime of the upper state is longer than that of the lower state, the relaxation of the lower level will occur at an earlier stage in the expansion process (Fig. 6.17b). Thus there will exist a fairly extensive region downstream from the expansion zone where there will be a population inversion. The length L of this region is roughly determined by the time taken for the N_2 molecule to transfer its excitation to the CO_2 molecule. The two laser mirrors are thus chosen to have a rectangular

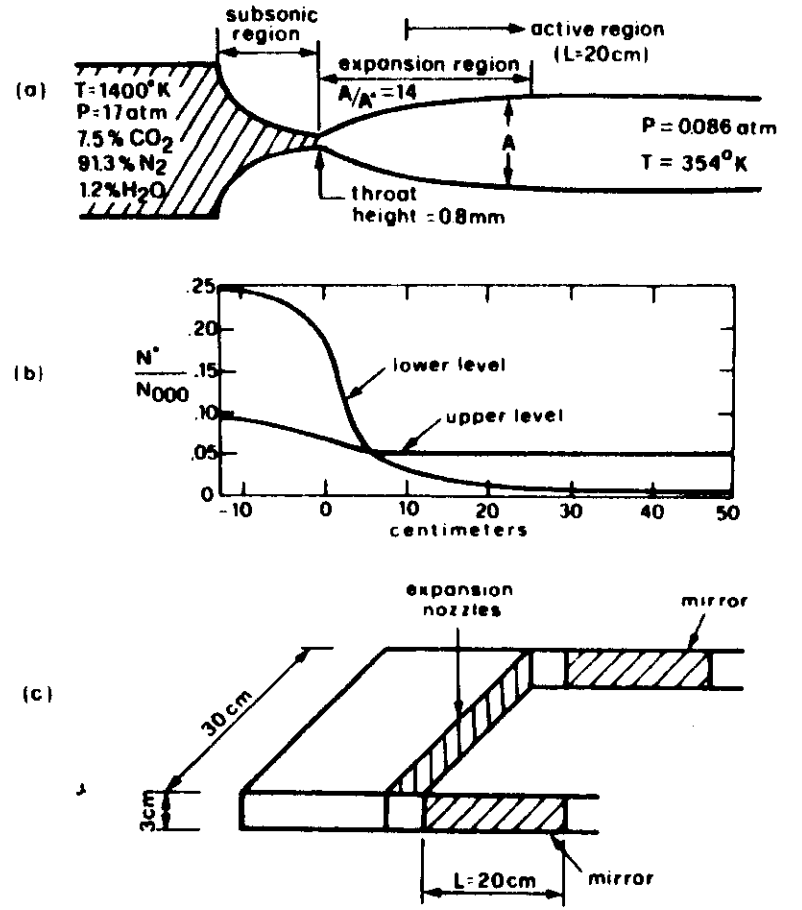

FIG. 6.17. Schematic illustration of the operation of a gas-dynamic CO_2 laser: (a) principle of the system, (b) spatial behavior of the population N^* for the upper and lower laser levels (normalized with respect to the population N_{000} of the ground level), (c) cavity geometry. Parts (a) and (b) have been reprinted by permission from *IEEE Spectrum*, Vol. 7, No. 11, November, 1970, pp. 51–58. Copyright 1970 by the Institute of Electrical and Electronics Engineers, Inc.

shape and are positioned as shown in Fig. 6.17c. This method of producing a population inversion will only work effectively if the expansion process reduces the temperature and pressure of the mixture in a time which is (i) short compared to the lifetime of the upper laser level and (ii) long compared to the lifetime of the lower laser level. To satisfy these conditions, expansion to supersonic velocities (Mach 4) is required. Finally we note

that the gas mixture is usually raised to its initial high temperature by combustion of appropriate fuels (e.g., combustion of CO and H_2 or of benzene, C_6H_6, and nitrous oxide, N_2O, thus automatically supplying a CO_2/H_2O ratio of 2 : 1).

Gas-dynamic CO_2 lasers have been reported which produce output power up to 80 kW with a chemical efficiency[†] of 1%. So far, this type of laser can only be operated continuously for a short time (a few seconds) because of the heating produced by the laser beam in some of the components (particularly the mirrors).

The category of gas lasers using vibrational–rotational transitions is obviously not limited to the CO_2 laser. Other examples which should be mentioned are the CO ($\lambda \simeq 5$ μm) and the HCN laser. The latter can oscillate at wavelengths as long as $\lambda = 773$ μm = 0.773 mm, thus reaching the millimeter wave region. The CO laser has attracted considerable interest on account of its high power and efficiency. Output powers in excess of 100 kW and efficiencies in excess of 60% have been demonstrated.[20] However, to achieve this sort of performance the gas mixture must be kept at cryogenic temperature (77–100°K). Laser action, in the 5 μm region, arises from several rotational–vibrational transitions [e.g., from $v'(11) \rightarrow v(10)$, to $v'(7) \rightarrow v(6)$ at $T = 77$°K] of the highly excited CO molecule.

Pumping of the CO vibrational levels is achieved by electron-impact excitation. Like the isoelectronic N_2 molecule, the CO molecule has an unusually large cross section for electron-impact excitation of its vibrational levels. Thus nearly 90% of the electron energy in a discharge can be converted into vibrational energy of CO molecules. Another important feature of the CO molecule is that V–V relaxation proceeds at a much faster rate than V–T relaxation (which is unusually low). As a consequence of this a non-Boltzmann population buildup in higher vibrational levels by a process known as "anharmonic pumping" plays a very important role.[‡] Although this phenomenon does not allow a *total* inversion in the vibrational population of a CO molecule, a situation known as *partial* inversion occurs. This is illustrated in Fig. 6.18 in which the rotational populations of two neighboring vibrational states are indicated. Although the total population for the two vibrational states is equal, an inversion is seen to exist in the two P transitions [$(J' = 5) \rightarrow (J = 6), (J' = 4) \rightarrow (J = 5)$] and two R-

[†] *Chemical efficiency* is defined as the ratio of laser output energy to the total chemical energy that can be produced by combustion of the fuel.

[‡] Anharmonic pumping arises from the process $CO(v = n) + CO(v = m) \rightarrow CO(v = n + 1) + CO(v = m - 1)$ which, due to the vibration anharmonicity, is favored when $n > m$. This process allows the first CO molecule to climb up the ladder of the vibrational levels with a resulting non-Boltzmann distribution of the population among these levels.

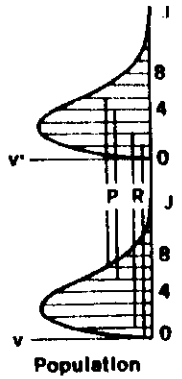

FIG. 6.18. Partial inversion between two vibrational transitions (V' and V'') having the same total population.

branch transitions indicated in the figure. Under conditions of partial inversion, laser action can thus take place and a new phenomenon, called *cascading*, plays an important role. The laser action depopulates a rotational level of the upper state and populates a rotational level of the lower vibrational state. The latter level can then accumulate enough population to result in population inversion with a rotational level of a still lower vibrational state. At the same time, the rotational level of the upper state may become sufficiently depopulated to result in population inversion with a rotational level of a still higher vibrational state. This process of cascading coupled with the very low V–T rate results in most of the vibrational energy being extracted as laser output energy. This, together with the very high excitation efficiency, accounts for the high efficiency of the CO laser. The low-temperature requirement arises from the need for very efficient anharmonic pumping. In fact, the overpopulation of the high vibrational levels compared to the Boltzmann distribution, and hence the degree of partial inversion, increases rapidly with decreasing translational temperature.

As in the case of the CO_2 laser, the CO laser has been operated with longitudinal flow, with *e*-beam pre-ionized pulsed TE, and with gas-dynamic excitation. The requirement of cryogenic temperatures has so far limited the commercial development of CO lasers.

6.3.3.2 *Vibronic Lasers*[21]

As a particularly relevant example of vibronic lasers, we will consider the N_2 laser. This laser has its most important oscillation at $\lambda = 337$ nm (UV), and belongs to the category of self-terminating lasers. The pulsed nitrogen laser is commonly used as a pump for dye lasers.

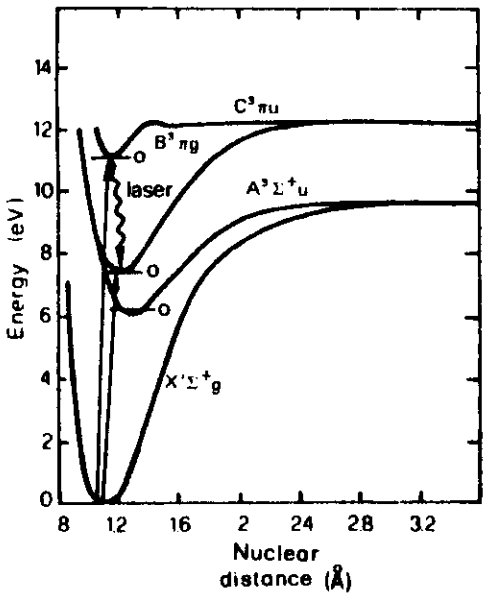

FIG. 6.19. Energy levels of the N_2 molecule. For simplicity only the lowest vibrational level ($v = 0$) is shown for each electronic state.

The relevant energy level scheme for the N_2 molecule is shown in Fig. 6.19. Laser action takes place in the so-called second positive system, i.e., in the transition from the $C^3\prod_u$ state (henceforth called the C state) to the $B^3\prod_g$ state (B state).[†] The excitation of the C state is believed to arise from electron-impact collisions with ground-state N_2 molecules. Since both C and B states are triplet states, transitions from the ground state are spin-forbidden. On the basis of the Franck–Condon principle, we can, however, expect that the excitation cross section to the $v = 0$ level of the C state will be larger than that to the $v = 0$ level of the B state. Compared to the ground state, the potential minimum of the B state is in fact shifted to larger internuclear separation than that of the C state. The lifetime (radiative) of the C state is 40 ns, while the lifetime of the B state is 10 μs. Clearly the laser cannot operate cw since condition (5.26) is not satisfied. It can, however, be excited on a pulsed basis provided the electrical pulse is appreciably shorter than 40 ns. Laser action takes place predominantly on several rotational lines of the $v''(0) \rightarrow v'(0)$ transition ($\lambda = 337.1$ nm). Besides being favored by the pumping process, as already mentioned, this transition in fact exhibits the largest Franck–Condon factor. Oscillation on

[†]Under different operating conditions laser action can also take place (in the near infrared, 0.74–1.23 μm) in the first positive system involving the $B^3\prod_g \rightarrow A^3\Sigma^+_u$ transition.

the $v''(1) \rightarrow v'(0)$ ($\lambda = 357.7$ nm) and on the $v''(0) \rightarrow v'(1)$ ($\lambda = 315.9$ nm) transitions also occur, although with lower intensity.

A possible configuration for a N_2 laser is shown schematically in Fig. 6.20a. Due to the high value of electric field required (~10 kV/cm at the typical operating pressure of $p \simeq 30$ Torr), a TE laser configuration is normally used. A fast discharge pulse (a few nanoseconds) is needed and a discharge circuit which achieves this, the so-called Blumlein configuration, is shown in Fig. 6.20. The transmission-line analog of this circuit is shown in Fig. 6.20b, where Z is the impedance of the discharge channel and Z_0 is the characteristic impedance of the line. If the line is initially charged to a voltage V, and if $Z = 2Z_0$, it can be shown that, upon closing the switch, a voltage pulse of value $V/2$ and duration $2L/c$ is produced across Z (c is the e.m. propagation velocity in the line). By making L short enough, the system of Fig. 6.20a can produce a short voltage pulse suitable for driving the N_2 laser.

Due to the high gain of this self-terminating transition, oscillation takes place in the form of amplified spontaneous emission. Thus the laser

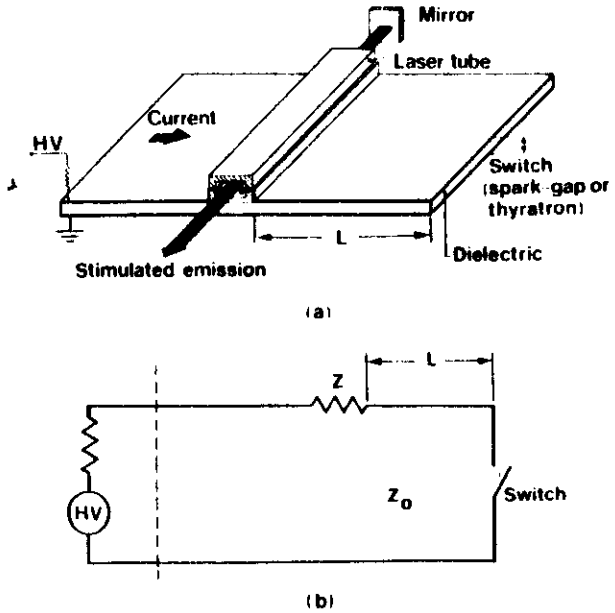

FIG. 6.20. (a) Blumlein pulse generator using a flat transmission line. The discharge channel may typically be 2 × 0.5 cm, the large dimension being along the discharge direction. (b) Transmission line analog of the Blumlein generator above.

can be operated without mirrors. However, usually, a single mirror is placed at one end of the cavity, since this reduces the threshold power [see (2.91*b*) and (2.91*d*)] and also provides a unidirectional output. In this way, the output beam divergence is also reduced and is given by the ratio of the transverse dimension of the discharge to twice the cavity length. With this type of laser, it is possible to obtain peak power up to $\sim$1 MW in pulses $\sim$10 ns wide with a pulse repetition rate up to 100 Hz. The repetition rate is limited by heating effects. More recently N_2 lasers working at atmospheric pressure have been developed. The problem of arcing is alleviated by further reducing (to $\sim$1 ns) the duration of the voltage pulse. Due to the increased gain per unit length and the fast discharge, this type of laser can give output pulses of duration 100–500 ps (100–200 kW peak power). No mirrors are used in this case. Such a laser, when used to pump dye lasers, can thus produce dye-laser pulses of duration well down into the subnanosecond range. These short pulses are useful for investigating relaxation processes in various materials.

There are, of course, other examples of vibronic lasers besides the N_2 laser. Of these other lasers we shall mention the H_2 laser. It oscillates on a series of lines around the wavelength $\lambda \simeq 160$ nm (Lyman band) and around $\lambda \simeq 116$ nm (Werner band). These wavelengths fall in the so-called vacuum ultraviolet (VUV). In fact, at these wavelengths, atmospheric absorption becomes so high that beam propagation must be done in a vacuum (or in a gas such as He). To provide the necessary fast discharge ($\sim$1 ns) a Blumlein configuration (Fig. 6.20a) is again used. This laser is also self-terminating, with its output being produced by amplified spontaneous emission.

It is interesting to note that the 116-nm wavelength is so far the shortest produced by laser action. The difficulty in getting to still shorter wavelengths (down to the x-ray region) is worth emphasizing at this point. From (3.25), (5.18), and (5.17) we find that the threshold pump power per unit volume is

$$\frac{dP_{th}}{dV} = \frac{1}{\eta_p}\hbar\omega_p W_{cp}(N_i - N_i) = \frac{\hbar\omega_p}{\eta_p}\frac{\gamma}{\sigma l \tau} \tag{6.12}$$

On the other hand, from (2.145) we find (for $\Delta\omega = 0$) that $(1/\sigma\tau) \propto \omega_0^2/g_i(0) \propto \omega_0^2\Delta\omega_0$. At frequencies in the UV and at moderate pressures we may assume that the linewidth $\Delta\omega_0$ is determined by Doppler broadening. Hence [see (2.113)] $\Delta\omega_0 \propto \omega_0$ and (dP/dV) increases as ω_0^4 (if we take $\omega_p \simeq \omega_0$). At still higher frequencies (x-ray region) the linewidth is determined by natural broadening since the value of radiative lifetime becomes very short. In this case $\Delta\omega_0 \propto \omega_0^3$ and (dP/dV) increases as ω_0^6. Due to the rapid increase of (dP/dV) with frequency, the required threshold power becomes very large. This explains why, despite many attempts, no one has so far succeeded in making an x-ray laser work.[†]

6.3.3.3 *Excimer Lasers*[22]

An interesting and important class of molecular lasers involving transitions between different electronic states is that of the excimer lasers.

Consider a diatomic molecule A_2 with potential energy curves as in Fig. 6.21 for the ground and excited states, respectively. Since the ground state is repulsive, the molecule does not exist in this state (i.e., species A only exists in the monomer form A in the ground state). Since, however, the potential energy curve for the excited state has a minimum, the molecule A_2 does exist in the excited state (i.e., species A exists in the dimer form A_2 in the excited state). Such a molecule A_2^* is called an "excimer" from a contraction of the words "excited dimer."

Now suppose a large number of excimers has somehow been created in a given volume. Laser action can then be produced on the transition between the upper (bound) state and the lower (free) state (bound–free transition). This is called an excimer laser. An excimer laser has two

[†]Recently, the achievement of a pulsed x-ray laser at the wavelength of 14 Å has been announced. The laser was pumped by the x rays produced by a small nuclear detonation (an experimental condition not so easily duplicated in everyone's laboratory!).

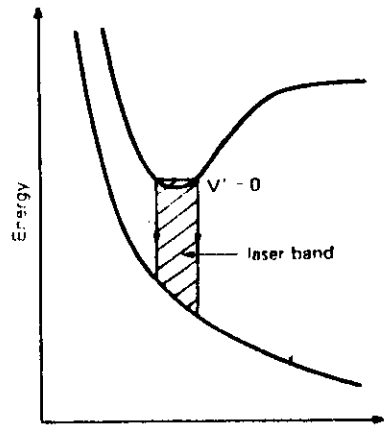

FIG. 6.21. Energy levels of an excimer laser.

peculiar but important properties, both due to the fact that the ground state is repulsive: (i) Once the molecule, after undergoing the laser transition, reaches the ground state, it immediately dissociates. This means that the lower laser level will always be empty. (ii) No well-defined rotational-vibrational transitions exist, and the transition is broad band. This allows the possibility of tunable laser radiation over this broad-band transition.

As a particularly relevant class of excimer lasers we will consider those in which a rare gas atom (e.g., Ar, Kr, Xe) is combined, in the excited state, with a halogen atom (e.g., F, Cl) to form a rare-gas-halide excimer.† Specific examples are ArF, (λ = 193 nm), KrF (λ = 248 nm), XeCl (λ = 308 nm), and XeF (λ = 351 nm), all oscillating in the UV. The reason why rare gas halides are readily formed in the excited state can be seen when one realizes that an excited rare gas becomes chemically similar to an alkali atom, and these are known to react readily with halogens. This analogy also indicates that the bonding in this excited state must be of ionic character: In the bonding process, the excited electron is transferred from the rare gas atom to the halogen atom. This bound state is therefore also referred to as a charge-transfer state.

The pumping mechanisms in a rare-gas-halide laser are rather complex since they involve several ionic species as well as excited atomic and molecular species. In KrF, for example (using Kr, F_2, and a buffer gas in the mixture), the following mechanisms play a very important role: (i) direct reaction of the excited rare gas with the halogen, viz.,

$$Kr^* + F_2 \rightarrow KrF^* + F \tag{6.13}$$

and (ii) dissociative attachment of an electron to the halogen (6.14*a*) followed by three-body recombination of the negative halogen ion (6.14*b*), i.e.,

$$e + F_2 \rightarrow F^- + F \tag{6.14a}$$

and

$$F^- + Kr^+ + M \rightarrow KrF^* + M \tag{6.14b}$$

where M is an atom of the buffer gas (Ar or He).‡

Rare-gas-halide excimer lasers can be pumped either by an electron beam or by an electrical discharge. In the latter case either *e*-beam or UV

†Strictly speaking these should not be called excimers since they involve unlike atoms. The words hetero-excimer or *exciplex* (from *excited state complex*) would perhaps be more appropriate in these cases. However, the word excimer is now widely used in this context and we will follow this usage.

‡The process in equation (6.14*b*) requires the presence of a buffer gas atom M since otherwise the momentum and the energy of the reacting partners (F and Kr) cannot both be conserved.

preionization techniques are used, the laser is pulsed, and its design is in many respects similar to that of a TEA CO_2 laser. The laser pulse length is of the order of a few tens of nanoseconds, being limited by the onset of discharge instabilities (arc formation). Average output powers up to 100 W, pulse repetition rates up to 1 kHz, and electrical efficiencies of 1% have been obtained. Excimer lasers are very promising for sophisticated photochemical processes, such as isotope separation, and for numerous other applications in which a strong and efficient UV source is required.

6.4 LIQUID LASERS (DYE LASERS)[23,24]

The liquid lasers we will be considering are those in which the active medium consists of solutions of certain organic dye compounds in liquids such as ethyl alcohol, methyl alcohol, or water. These dyes usually belong to one of the following classes: (i) polymethine dyes (0.7–1 μm), (ii) xanthene dyes (0.5–0.7 μm), (iii) coumarin dyes (0.4–0.5 μm), and (iv) scintillator dyes ($\lambda < 0.4$ μm). By virtue of their wavelength tunability, wide spectral coverage, and simplicity, organic dye lasers are playing an increasingly important role in various fields of application (from spectroscopy to photochemistry).

6.4.1 Photophysical Properties of Organic Dyes

Organic dyes are large and complicated molecular systems† containing conjugated double bonds. Usually they have strong absorption bands in the UV or visible range of the spectrum, and when excited by light of appropriate wavelength, they display intense broad-band fluorescence spectra, such as that shown in Fig. 6.22 for Rhodamine 6G in ethanol solution.

A simple understanding of the energy levels of a dye molecule can be obtained using the so-called free-electron model. We will illustrate this by considering the case of the cyanine dye shown in Fig. 6.23a. The π-

†As an example, the structural formula for the widely-used dye Rhodamine 6G (xanthene dye) is

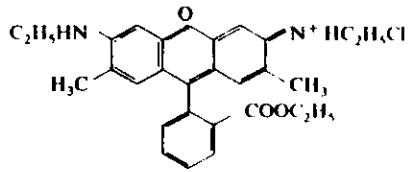

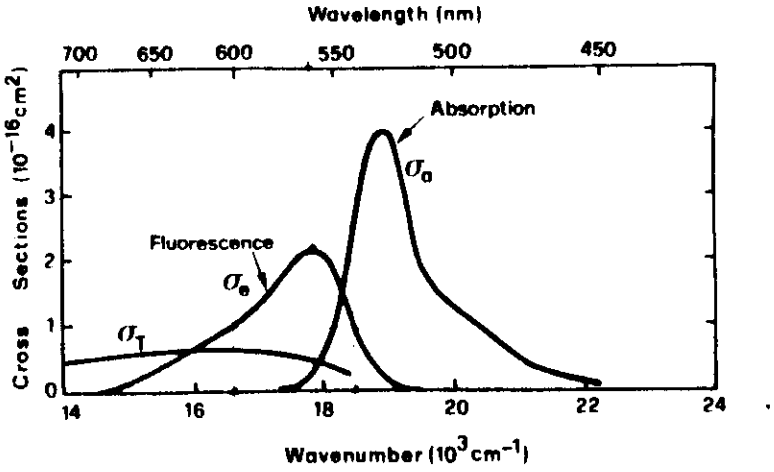

FIG. 6.22. Absorption cross section σ_a, stimulated-emission cross section σ_e (singlet–singlet transition), and absorption cross section σ_T (triplet–triplet transition) for an ethanol solution of Rhodamine 6G.

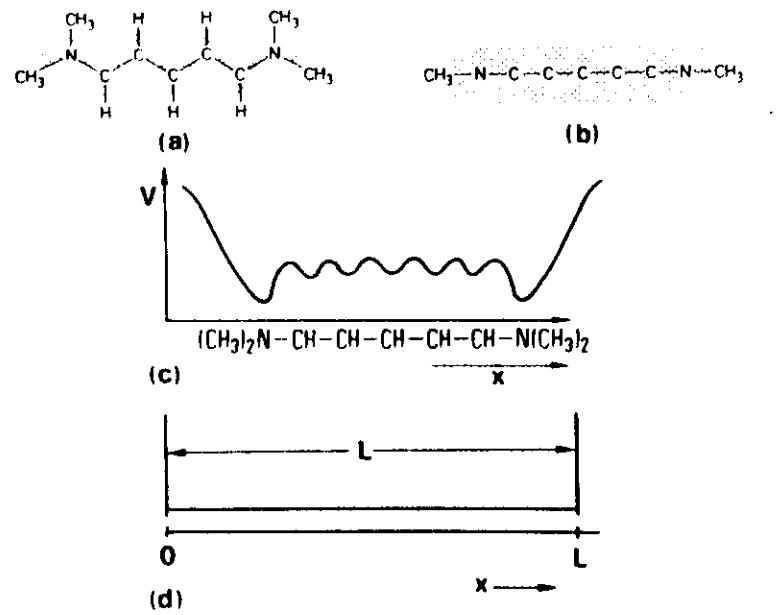

FIG. 6.23. Free-electron model to explain the electronic energy levels of a dye molecule [after Forsterling and Kuhn[361]].

electrons of the carbon atoms form two planar distributions, one above and one below the plane of the molecule (Fig. 6.23b). The electronic states of the molecule originate from this π-electron distribution. In the free-electron model, these π-electrons are assumed to move freely within their planar distributions, limited only by the repulsive potential of the group at each end of the dye. The energy levels of the electrons are therefore simply those of a free electron in a potential well of the form shown in Fig. 6.23c. If this well is approximated by a rectangular one (Fig. 6.23d), the energy levels are well known and given by $E_n = h^2n^2/8mL^2$ where n is an integer, m is the electron m[illegible] and L is the length of the well. It is important to note, at this point, that dye molecules have an even number of electrons in the π-electron cloud.† If we let the number of these electrons be $2N$, the lowest energy state of the molecule will correspond to the situation where these electrons are occupying the lowest N energy levels. Each level can in fact be occupied by two electrons with opposite spin. This molecular state will thus have zero spin angular momentums (singlet state) and is labeled S_0 in Fig. 6.24. In the same figure the highest occupied level and the next (empty) one above it are indicated by two squares one above the other. The first excited singlet state (labeled S_1 in the figure) is then obtained by

†Molecular systems with unpaired electrons are known as radicals and they tend to react readily, thus forming a system with paired electrons.

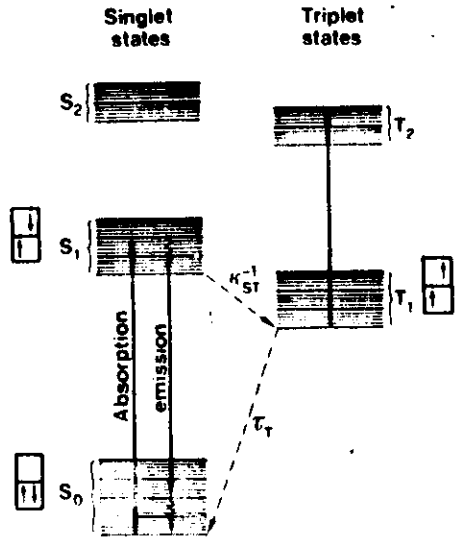

FIG. 6.24. Typical energy levels for a dye in solution. The singlet and triplet levels are shown in separate columns.

promoting one of the two highest-lying electrons, without flipping its spin, to the next level up. If the spin is flipped, the resulting state is a triplet state (total spin $S = 1$, labeled T_1 in the figure). Excited singlet (S_2) and triplet (T_2) states result when the electron is further promoted to the next level, and so on. Note that in Fig. 6.24 each electronic state is actually made up of a set of vibrational levels (the heavier lines in the figure) and rotational levels (the lighter lines). The separation between vibrational levels is typically 1400–1700 cm^{-1}, whereas the separation of rotational levels is typically 100 times less. Since the line broadening mechanisms are much more important in liquids than in solids, the rotational lines are not resolved and therefore give rise to a continuum of levels between the vibrational levels.

We now look at what happens when the molecule is subjected to electromagnetic radiation. First, we recall that the selection rules require that $\Delta S = 0$. Hence singlet–singlet transitions are allowed, whereas singlet–triplet transitions are forbidden. Therefore, the interaction with electromagnetic radiation can raise the molecule from the ground level S_0 to one of the vibrational levels of the S_1 level. Since the rotational and vibrational levels are unresolved, the absorption spectrum will show a broad and featureless transition (see, for example, Fig. 6.22). Note that an important characteristic of these dyes is that they have a very large dipole matrix element μ. This is because the π-electrons are free to move over a distance comparable to the molecular dimension a, and since a is quite large it follows that μ is large ($\mu \simeq ea$). It then follows that the absorption cross section σ, which is proportional to μ^2, is also large ($\sim 10^{-16}$ cm^2). Once in the excited state the molecule decays in a very short time (nonradiative decay, $\tau_{nr} \simeq 10^{-12}$ s) to the lowest vibrational state of the S_1 level.[†] From there it decays radiatively to some vibrational level of S_0 (*fluorescence*). The transition probability will be determined by the appropriate Franck–Condon factors. It is therefore clear from what has already been said (see also Fig. 2.22) that the fluorescent emission will take the form of a broad and featureless band shifted to the long-wavelength side of the absorption band (see Fig. 6.22). Having dropped to an excited rotational–vibrational state of the ground level S_0, the molecule will then return to the lowest vibrational level by another very fast (of the order of picoseconds) nonradiative decay. Note that, when the molecule is in the lowest level of S_1, it can also decay to level T_1. This process is called *intersystem crossing* and is caused by collisions. Similarly the transition $T_1 \rightarrow S_0$ takes place mainly by

[†]More precisely, thermalization among the rotational-vibrational levels of the S_1 state will occur.

way of collisions but partly also by a radiative process (the transition $T_1 \rightarrow S_0$ is prohibited radiatively as mentioned above). This radiation is called *phosphorescence*. We will characterize these three decay processes by the following three constants: (i) τ_{sp}, spontaneous-emission lifetime of level S_1, (ii) k_{ST} intersystem crossing rate (s^{-1}) between singlet and triplet systems, and (iii) τ_T, lifetime of the T_1 level. If we call τ the lifetime of the S_1 level, then we have [see (2.93)]

$$\frac{1}{\tau} = \frac{1}{\tau_{sp}} + k_{ST} \tag{6.15}$$

Due to the large value of the dipole matrix element μ, the radiative lifetime τ_{sp} is very short (a few nanoseconds). Since k_{ST}^{-1} is usually much longer ($\sim$100 ns), it follows that most of the molecules decay from level S_1 by fluorescence. The fluorescence quantum yield (number of photons emitted by fluorescence divided by number of atoms put into S_1) is therefore nearly unity. In fact, one has [see (2.96)]

$$\phi = \tau/\tau_{sp} \tag{6.16}$$

The triplet lifetime τ_T depends on the experimental conditions and particularly on the amount of dissolved oxygen in the solution. The lifetime can range from 10^{-7} s in an oxygen-saturated solution to 10^{-3} s or more in a solution which has been deoxygenated.

6.4.2 Characteristics of Dye Lasers

From what has been said it is quite reasonable to expect these materials to be capable of exhibiting laser action at the fluorescence wavelengths. In fact, the fast nonradiative decay within the excited single-state S_1 populates the upper laser level very effectively while the fast nonradiative decay within the ground state is effective in depopulating the lower laser level. Note also that the dye solution is quite transparent to the fluorescence wavelengths (i.e., the corresponding absorption cross section σ_a is very low, see for example Fig. 6.22). In fact it was quite late in the general development of laser devices before the first dye laser was operated (1966),[25] and we now look at some reasons for this. One problem which presents itself is the very short lifetime τ of the S_1 state since the required pump power is inversely proportional to τ. Although this is to some extent compensated by the comparatively large value of the cross section, the product $\sigma\tau$ [recall that threshold pump power is $\propto (\sigma\tau)^{-1}$, see (6.12)] is still about three orders of magnitude smaller than for solid-state lasers such as

Nd:YAG. A second problem arises as a consequence of intersystem crossing. If, in fact, τ_T is long compared to k_{ST}^{-1}, then molecules accumulate in the triplet state T_1. This introduces absorption through the $T_1 \rightarrow T_2$ transition (which is optically allowed). Unfortunately, this absorption tends to occur in the same wavelength region as the fluorescence (see again, for example, Fig. 6.22), and is therefore a serious obstacle to laser action. It can be shown, in fact, that continuous laser action is possible only if τ_T is less than some particular value, depending on the characteristics of the dye material. To derive this result we first note that the fluorescence emission curve of the dye (see Fig. 6.22) can be described in terms of the stimulated emission cross section σ_e. Thus, if N_2 is the total population of the S_1 state, the corresponding (unsaturated) gain, at the given wavelength to which σ_e refers, is $\exp(N_2\sigma_e l)$, where l is the length of the active material. If we now let N_T be the population in the triplet state T_1, a necessary condition for laser action is that the gain due to stimulated emission exceed the loss due to triplet–triplet absorption, i.e.,

$$\sigma_e N_2 > \sigma_T N_T \tag{6.17}$$

In the steady state, the rate of decay of triplet population N_T/τ_T must equal the rate of increase due to intersystem crossing $k_{ST}N_2$, i.e.,

$$N_T = k_{ST}\tau_T N_2 \tag{6.18}$$

Combining (6.17) and (6.18), we get

$$\tau_T < \sigma_e/\sigma_T k_{ST} \tag{6.19}$$

which is a necessary condition for cw laser action [i.e., in a sense equivalent to (5.26)]. If this condition is not satisfied, the dye laser can only operate in a pulsed regime. In this case, the duration of the pump pulse must be short enough to ensure that an excessive population does not accumulate in the triplet state. Finally, a third crucial problem comes from the presence of thermal gradients produced in the liquid by the pump. These tend to produce refractive-index gradients which prevent laser action. These gradients produce effects which are similar in some respects to those due to intersystem crossing. Both of these processes tend to cause laser action to terminate after the pump has been applied for a certain length of time. Fortunately, however, as already mentioned, τ_T can be reduced if certain substances (e.g., oxygen) are added to the solution, while thermal effects can also be reduced with a suitable experimental arrangement.

Pulsed laser action has been obtained from very many different dyes by using one of the following pumping schemes: (i) fast flashlamps (with a risetime of $< 1\ \mu s$), (ii) a short light pulse from another laser. The N_2 laser in particular is very frequently used for this application. Its UV output is suitable for pumping many dyes that oscillate in the visible range. This pumping scheme is particularly efficient: Very high gains and a conversion efficiency (from UV to visible light) of the order of 10% have been achieved. The efficiency of the N_2 laser is rather low, however ($\sim$0.2%). For this reason, excimer lasers (in particular KrF and XeF) are being used increasingly as pumps for dye lasers. For both N_2 and excimer laser pumping, a transverse pump configuration (i.e., direction of the pump beam orthogonal to the resonator axis) is used (Fig. 6.25a). The telescope shown in the figure serves to enlarge the beam on the echelle grating (used as a wavelength-selective element, see Fig. 5.7), thus increasing its resolving power. The Fabry–Perot etalon (see also Fig. 5.8) is used for fine tuning of the output wavelength. Continuous laser action has been obtained in a number of laser dyes covering the entire visible range. Pumping is provided by another cw laser (usually an Ar^+ laser), and a longitudinal (or near longitudinal) pump configuration such as that in Fig. 6.25b is commonly used. Note the presence of the dispersive prism in the laser cavity which serves the double purpose of (i) tuning the laser wavelength (see again Fig. 5.7) and (ii) allowing the pump laser beam to be physically separated from the dye laser beam in the region indicated in the figure. Since the pump beam comes in around the side of the dye laser mirror, rather than through it, one avoids the need for special mirrors which are transparent to the pump and highly reflecting for the dye wavelengths. A rather interesting configuration for single-longitudinal-mode cw dye lasers is the ring cavity shown in Fig. 6.26. Pumping is again provided by an ion laser, and the dye

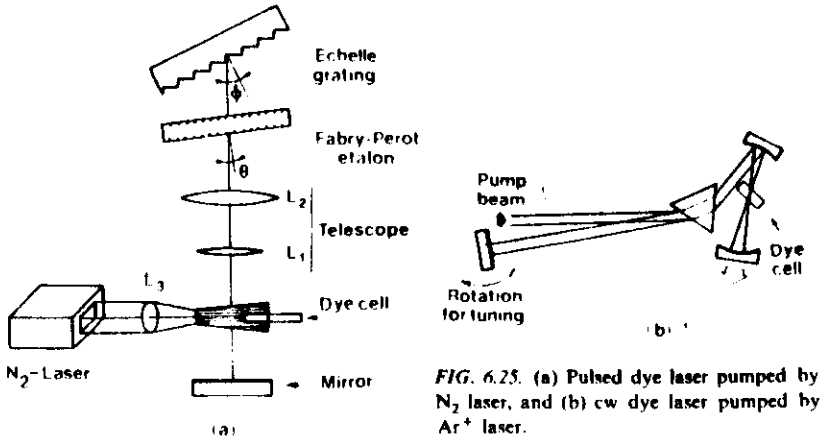

FIG. 6.25. (a) Pulsed dye laser pumped by N_2 laser, and (b) cw dye laser pumped by Ar^+ laser.

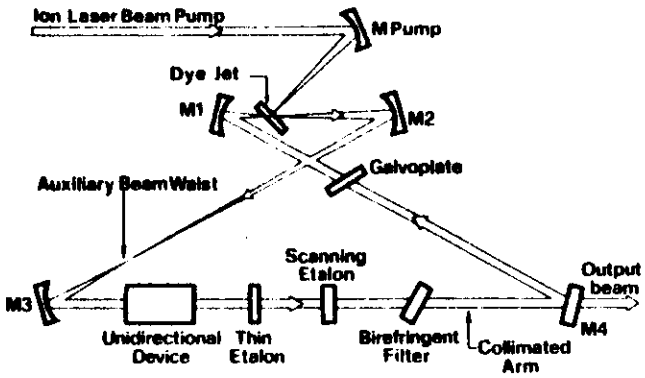

FIG. 6.26 High power single longitudinal mode ring dye laser.

is circulated by means of a liquid jet system. Single-longitudinal-mode oscillation and frequency scanning are achieved by the combination of birefringent filter, scanning etalon, and thin Fabry–Perot etalon. The special feature of this cavity is that, with the help of the unidirectional device, the laser beam can only travel in one sense around the ring cavity (indicated by the arrows in the figure). Thus there is no standing wave formed in the cavity and, in particular, within the dye medium. Therefore the phenomenon of spatial hole burning does not occur and this has two consequences: (i) Oscillation on a single longitudinal mode is much easier to obtain as can be understood by referring to the discussion in connection with Fig. 5.6. (ii) Higher output power is available in this single mode since now the whole of the active material (rather than just those regions around the maxima of the standing-wave pattern) contributes to the laser output. As a result of this, output powers have been obtained which are as much as an order of magnitude greater than those from conventional single-mode dye lasers (e.g., of the type of Fig. 6.25b).

Average output powers up to 100 W with an efficiency somewhat less than 1% have been obtained with flashlamp-pumped dye lasers. A very interesting property of dye lasers is their wide oscillation bandwidth ($\sim$10 nm). Tuning of the output wavelength over this bandwidth can therefore be achieved using wavelength-selecting cavities such as those of Fig. 5.7. A large oscillation bandwidth is also very important for mode-locked operation. Continuous-wave (Ar^+ laser-pumped) mode-locked dye lasers in a ring configuration have been operated with output pulse durations as short as $\sim$0.03 ps. These are the shortest pulses so far obtained from lasers.

Dye lasers are now widely used in many scientific and technological applications where wavelength tunability or pulses of short duration are

required. Photodegradation of the dye due to the pump light remains an inconvenient feature of these lasers.

6.5 CHEMICAL LASERS[26,27]

A *chemical laser* is usually defined as one in which the population inversion is "directly" produced by a chemical reaction. According to this definition, the gas-dynamic type of CO_2 laser cannot be regarded as a chemical laser. Chemical lasers usually involve a chemical reaction between gaseous elements. In this case, a large proportion of the reaction energy is left in the form of vibrational energy of the molecules. The laser transitions are therefore often of vibrational–rotational type (the only notable exception being perhaps the photochemical-dissociation laser to be described later on), and the corresponding wavelengths lie at present between 3 and 10 μm. These lasers are interesting for two main reasons: (i) They provide an interesting example of direct conversion of chemical energy into electromagnetic energy. (ii) Since the amount of energy available in a chemical reaction is very large,† one can expect high output powers.

As an illustrative example of chemical lasers we will consider the HF laser. This laser oscillates over several rotational–vibrational lines in the 2.6 to 3.3 μm band and gives cw output powers up to 10 kW and pulsed energies up to a few kilojoules with a chemical efficiency up to $\sim$10%.

The main pumping mechanism for the HF laser comes from the chemical reaction

$$F + H_2 \rightarrow HF^* + H \tag{6.20}$$

Since the heat of reaction is 31.6 kcal/mole, the HF molecule can be left in an excited state as high as the $v = 3$ vibrational level (see Fig. 6.27). As a consequence of the different rates of decay to the various vibrational levels, the $v = 2$ level has by far the greatest population, and a large population inversion builds up on the $(v' = 2) \rightarrow (v = 1)$ transition. It can be seen from the figure that more than 60% of the reaction energy is released as vibrational energy. The reason why, after chemical reaction, the HF molecule is left in an excited state can be understood in a simple way. Consider the reaction given in equation (6.20). On account of the high electron affinity of F, at large distances the F–H_2 interaction is strongly attractive and leads to a considerable polarization of the H_2 charge distribution. Since the electron is light, the HF bond can form before the proton has adjusted

†For example, a mixture of H_2, F_2, and other substances (16% of H_2 and F_2 at atmospheric pressure) has a heat of reaction equal to 2000 J/liter of which 1000 J is left as vibrational energy.

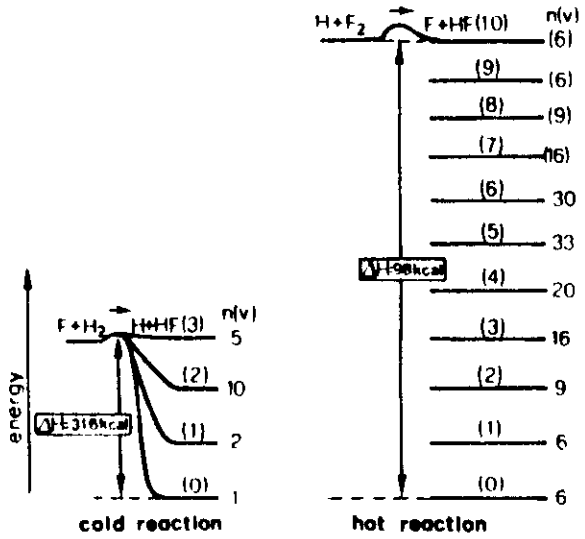

FIG. 6.27 Pumping of the vibrational levels of the HF molecule by the two reactions, $F + H_2 \rightarrow H + HF^*$ and $H + F_2 \rightarrow F + HF^*$. The relative populations $n(v)$ produced in this way are also shown.

to the internuclear separation appropriate to the HF ground electronic state. Thus, there is a considerable probability that the proton, after reaction, will be found at a distance which is greater than the equilibrium distance of the HF bond. This therefore leads, classically, to a vibrational motion.

Note that, for the chemical reaction in equation (6.20) to occur, atomic fluorine must be present. This is produced by dissociation of some suitable fluorine-donating molecule such as SF_6 or molecular F_2. Dissociation may be achieved in several ways, e.g., by electron collision in an electrical discharge ($SF_6 + e \rightarrow SF_5 + F + e$). When molecular fluorine is used, the undissociated F_2 molecules can react with atomic hydrogen [itself produced by reaction (6.20)] to yield

$$H + F_2 \rightarrow HF^* + F \qquad (6.21)$$

The atomic fluorine produced in this way can then take part again in reaction (6.20). This leads to a chain reaction in which the number of excited HF molecules can greatly exceed the number of fluorine atoms produced initially. Note that the chemical energy of reaction (6.21) (98 kcal/mole) is substantially larger than that of (6.20). This can result in excitation up to the $v = 10$ vibrational level of the HF molecule (Fig. 6.27). Reaction (6.21) therefore helps to establish a population inversion between various vibrational levels of the HF molecule. From what has just been said, it would seem that molecular fluorine might be more suitable than SF_6 for use in an HF laser. However, the $H_2 + F_2$ mixture is more difficult to handle than the $H_2 + SF_6$ mixture, and it may even become explosive.

HF lasers can be made to operate either pulsed or cw. In pulsed lasers, atomic fluorine is produced by collisions between the fluorine donors and electrons generated either by an electrical discharge or by an auxiliary electron-beam machine. Where an electrical discharge is used, the pump configuration is similar to that of a TEA CO_2 laser, and UV pre-ionization is often used to ensure a more uniform discharge. When molecular fluorine is used as a reactant, a chain reaction is established, and the laser output energy can appreciably exceed the energy of either the electrical discharge or e-beam. In a cw laser, fluorine is thermally dissociated by an arc jet heater and then expanded through supersonic nozzles (to ~Mach 4). Molecular hydrogen is mixed in downstream and reacts according to (6.20) (Fig. 6.28). For high-power or high-energy lasers, unstable resonators are often used.

Laser action takes place on several vibrational transitions, from $1 \rightarrow 0$ up to $6 \rightarrow 5$ ($\lambda = 2.7$–3.3 μm) and on several rotational lines within each vibrational transition. As already discussed in the case of the CO laser, there are two reasons why oscillation can occur on so many lines, namely: (i) The phenomenon of cascading. If in fact the $2 \rightarrow 1$ transition (usually the strongest) lases, the population of level 2 will be depleted and will accumulate in level 1. Consequently laser action on $3 \rightarrow 2$ and $1 \rightarrow 0$ transition may now occur. (ii) The phenomenon of partial inversion (see Fig. 6.18) in which there may be a population inversion between some rotational lines even when no inversion exists between the overall populations of the corresponding vibrational levels.

Besides the HF laser, mention should be made of the DF, HCl, and HBr lasers which operate on similar schemes to HF and oscillate in the 3.5–5 μm range. This range is interesting since it is a spectral region where

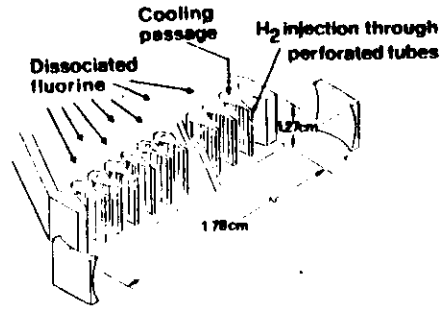

FIG. 6.28 Supersonic-diffusion HF chemical laser [after Chester[20]].

the atmospheric transmission is good. As already mentioned, chemical lasers of this type can give large output powers (or energies) with good chemical efficiency. Safety problems (F_2 is perhaps the most corrosive and reactive element known) greatly limit the applicability of these lasers, however. Although electrical-discharge lasers (using SF_6) are commercially available, the most important area of use for these lasers seems to be in high-power military applications.

As a second example of a chemical laser we will briefly mention the atomic iodine laser.[28] It belongs to the category of photochemical-dissociation (or photodissociation) lasers. Atomic iodine is in fact produced by photodissociation of either CH_3I or CF_3I or, more recently, C_3F_7I. When light ($\sim$300 nm) from a powerful flashlamp is absorbed by one of the above molecules, photodissociation leads to production of atomic iodine in the $^2P_{1/2}$ excited state at a greater rate than in the $^2P_{3/2}$ ground state. Thus laser oscillation takes place on the $^2P_{1/2} \rightarrow {}^2P_{3/2}$ line ($\lambda = 1.315$ μm). This line is forbidden as an electric-dipole transition but allowed as a magnetic-dipole transition. Since the corresponding spontaneous-emission lifetime is very long (in the millisecond range), the lifetime of the $^2P_{1/2}$ state is essentially governed by collisional deactivation. The lifetime of the $^2P_{3/2}$ ground state is governed by the three-body recombination process $I(^2P_{3/2}) + I(^2P_{3/2}) + M \rightarrow I_2 + M$, where M is another atom or molecule in the gas mixture (He, I_2). This lifetime is typically 100 μs. The characteristics of an iodine laser fall somewhat in between those typical of a gas laser and those typical of an optically pumped solid-state laser. The iodine, being a gas, must be contained in a glass tube (Fig. 6.1) just as for any other gas laser. However, the iodine laser is similar to solid-state lasers in two respects: (i) It is pumped by a flash in a geometrical configuration similar to those used for solid-state lasers (Fig. 3.2). (ii) As in the case of ruby and Nd^{3+} lasers, the laser line is a forbidden electric-dipole transition. This last property is particularly relevant. It means that the iodine laser has a long upper-state lifetime, and hence it can build up a large population inversion. This places the iodine laser (together with the Nd:glass and CO_2 lasers) among the most interesting systems for high-energy (> 500 J) laser output.

6.6 SEMICONDUCTOR LASERS[29]

So far, we have only discussed atomic and molecular systems, whose energy levels are associated with localized wave functions, i.e., belong to single atoms or molecules. We will now consider the case of semiconductors for which it is no longer possible to talk about the wavefunction of an individual atom; it is necessary instead to deal with a wavefunction relating to the crystal as a whole. Likewise, one can no longer talk of energy levels of individual atoms.

6.6.1 Photophysical Properties of Semiconductor Lasers

The energy-level scheme for an idealized semiconductor is shown in Fig. 6.29. The energy-level spectrum consists of very broad bands: These are the valence band V and the conduction band C, separated by a region of forbidden energies (the band gap). Each band actually consists of a large number of very closely spaced energy states. According to the Pauli exclusion principle, there can be just two electrons (with opposite spin) occupying each energy state. Accordingly, the probability of occupation $f(E)$ of a given state of energy E is given by Fermi-Dirac statistics rather than by Maxwell-Boltzmann statistics. Thus

$$f(E) = \{1 + \exp[(E - F)/kT]\}^{-1} \tag{6.22}$$

where F is the energy of the so-called Fermi level. This level has the following physical significance: when $T \rightarrow 0$, one has

$$\begin{aligned} f &= 1 \quad (\text{for } E < F) \\ f &= 0 \quad (\text{for } E > F) \end{aligned} \tag{6.23}$$

so that this level represents the boundary between fully occupied and completely empty levels at $T = 0°K$. For nondegenerate semiconductors the Fermi level is situated inside the band gap (see Fig. 6.29). Therefore, at $T = 0°K$ the valence band will be completely full, and the conduction band, completely empty. It can be shown that, under these conditions, the semiconductor will not conduct, and it is therefore an insulator. Note also that the Fermi level has also another physical meaning: At any temperature one has $f(F) = 1/2$.

Having made these preliminary remarks, we can now begin to describe the principles of operation of a semiconductor laser. For simplicity, we will

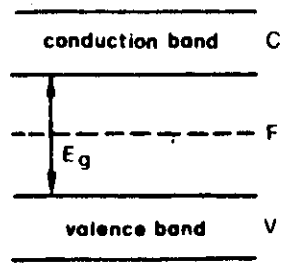

FIG. 6.29. Valence band, conduction band, and Fermi level of a semiconductor.

first assume that the semiconductor is at $T = 0°K$ (see Fig. 6.30a, in which the hatched area corresponds to completely full energy states). Now we suppose that electrons are somehow raised from the valence band to the conduction band. After a very short time ($\sim 10^{-13}$ s) the electrons in the conduction band will have dropped to the lowest levels in that band, and any electrons near the top of the valence band will also have dropped to the lowest unoccupied levels, thus leaving the top of the valence band full of "holes." This means that there is then a population inversion between the valence and conduction bands (Fig. 6.30b). The electrons in the conduction band fall back into the valence band (i.e., they recombine with holes), emitting a photon in the process (recombination radiation). Given a population inversion between conduction and valence bands as shown in Fig. 6.30b, the process of stimulated emission of recombination radiation will produce laser oscillation when the semiconductor is placed in a suitable resonator. From Fig. 6.30b it is seen that the frequency of the emitted radiation must satisfy the condition

$$E_g < h\nu < F_c - F_v \tag{6.24}$$

which establishes the gain bandwidth of the semiconductor.

We now consider the situation where the semiconductor is held at a temperature $T > 0$. Referring again to Fig. 6.30b, we note that, although the semiconductor as a whole is not in thermal equilibrium, nevertheless equilibrium will be reached within a single band in a very short time. One can therefore talk of occupation probabilities f_v and f_c for the valence and conduction bands separately, where f_v and f_c are given by expressions of the same form as (6.22), namely,

$$f_v = \{1 + \exp[(E - F_v)/kT]\}^{-1} \tag{6.25a}$$

$$f_c = \{1 + \exp[(E - F_c)/kT]\}^{-1} \tag{6.25b}$$

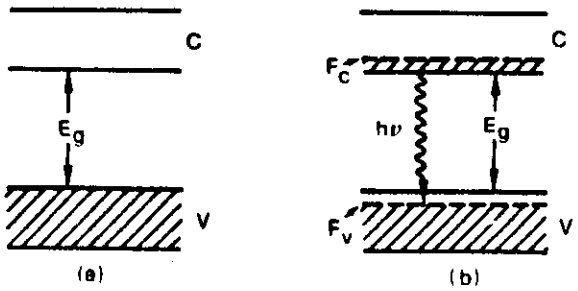

FIG. 6.30. Principle of operation of a semiconductor laser.

where F_v and F_c are the energies of the so-called quasi-Fermi levels of the valence and conduction bands respectively. From (6.25) and from our preliminary remarks, it is seen that when, for instance, $T = 0°K$, these levels separate the zones of fully occupied and completely empty levels for each band. Obviously the values of F_v and F_c depend on the number of electrons raised to the conduction band by the pumping process. Having introduced the concept of quasi-Fermi levels, we can readily obtain a necessary condition for laser action by imposing the requirement that the number of stimulated-emission events must be greater than the number of absorption events (the excess being necessary to overcome cavity losses). Both of these processes are proportional to the product of the number of photons present in the cavity and the B coefficient for the transition. On the other hand, the stimulated-emission rate will also be proportional to the product of the probability of occupation of the upper level with the probability of nonoccupation of the lower level, whereas the absorption rate will be proportional to the product of the occupation probability of the lower level with the probability of nonoccupation of the upper level. Therefore, to get stimulated emission, we must satisfy

$$Bq[f_c(1 - f_v) - f_v(1 - f_c)] > 0 \tag{6.26}$$

This inequality means that $f_c > f_v$. From (6.25) this implies

$$F_c - F_v > E_2 - E_1 = h\nu \tag{6.27}$$

where E_2 and E_1 are the upper- and lower-level energies respectively. We have thus rederived one of the two relations which were previously found with an intuitive approach for $T = 0°K$ [see (6.24)]. This derivation, however, shows that the relationship is valid for any temperature (as long as the concept of quasi-Fermi levels remains valid). Furthermore it has been shown that equation (6.27) is a consequence of the requirement that stimulated emission processes must exceed stimulated absorption processes. In this respect equation (6.27) is seen to be equivalent to the condition (5.26) established for a four-level laser.

6.6.2 *Characteristics of Semiconductor Lasers*

The pumping process in a semiconductor laser is usually achieved by preparing the semiconductor in the form of a p–n junction diode with highly degenerate p-type and n-type regions, i.e., heavily doped (donor or acceptor concentration greater than 10^{18} atoms/cm^3). It will be seen that in this way the inversion is produced in the junction region.

As a first example of a junction laser we will consider the situation where the p-type and n-type materials are the same (e.g., GaAs) and are

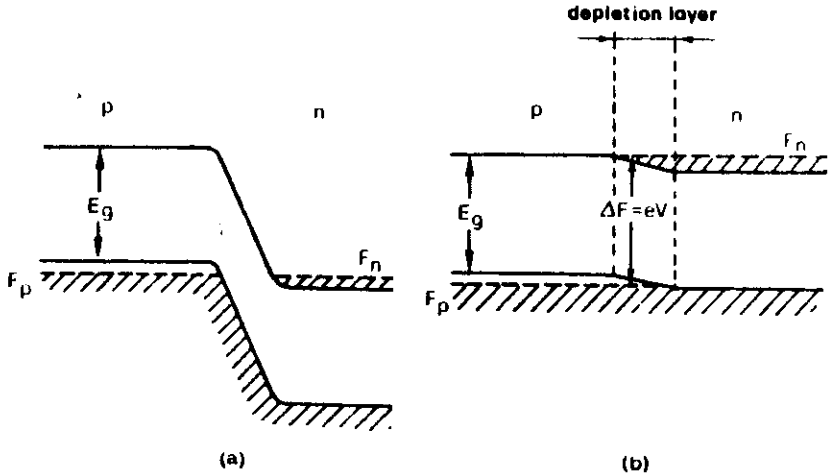

FIG. 6.31. Principle of operation of a p–n junction semiconductor laser with (a) zero bias and (b) forward bias.

joined directly to form the junction (which is therefore called a homojunction). The first semiconductor laser to work was of this type.[30,31] The operating principles of a diode constructed in this way are illustrated in Fig. 6.31. Since the materials are very heavily doped, the Fermi level F_p of the p-type semiconductor falls within the valence band, and the Fermi level F_n of the n-type semiconductor falls within the conduction band. It can be shown that, with no voltage applied, the two Fermi levels lie on the same horizontal line (Fig. 6.31a), i.e., they have the same energy. When a voltage V is applied, the two levels become separated by an amount given by

$$\Delta F = eV \tag{6.28}$$

So, if the diode is forward biased, the energy levels will then be as shown in Fig. 6.31b. We see from the figure that a population inversion has been produced in the so-called "depletion layer" of the p–n junction. What the forward bias achieves essentially is the injection into the depletion layer of electrons from the conduction band of the n-type material and holes from the valence band of the p-type material. Finally, we note that since $\Delta F \simeq E_g$, where E_g is the band gap, it follows from (6.28) that $V \simeq E_g/e$. For a GaAs laser this means $V \simeq 1.5$ V.

Figure 6.32 shows a schematic diagram of a p–n junction laser, the shaded region being the depletion layer. It is seen that the diode has small dimensions. The thickness of the depletion region is usually very small (0.1

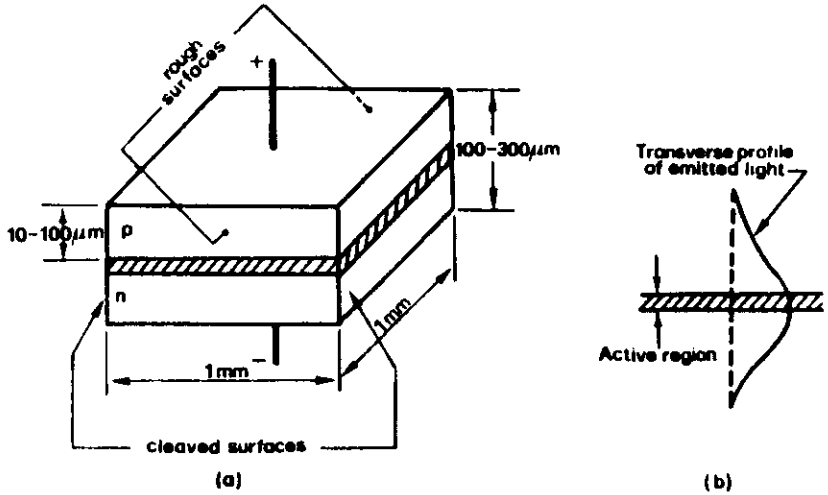

FIG. 6.32. (a) Schematic diagram of a semiconductor laser; (b) transverse distribution of light intensity.

μm). To obtain laser action, two end faces are made parallel, usually by cleavage along crystal planes. The other two are left with a rough finish to suppress oscillation in unwanted directions. Often the two surfaces are not provided with reflecting coatings: In fact, since the refractive index of a semiconductor is very large, there is already a sufficiently high reflectivity (~35%) for the semiconductor–air interface. The active region consists of a layer of thickness ~1 μm, i.e., somewhat wider than the depletion region. Due to diffraction the transverse dimension of the beam is in turn much greater (~40 μm) than the width of the active region (Fig. 6.32b). The laser beam therefore extends well into the p and n regions. However, since the transverse dimensions of the beam are still very small, the output beam ends up with a rather large divergence (a few degrees). Finally we point out that, at room temperature, the threshold current density for a homojunction laser is quite high (~10^5 A/cm^2 for GaAs). This is due to the high losses of the cavity mode since it extends far into the p and n regions (where absorption rather than gain is dominant). This current density, however, decreases rapidly with decreased operating temperature [approximately as $\exp(T/T_0)$, where the value of T_0 and the range of validity of the expression vary from one semiconductor to another]. This is a result of the fact that, as the temperature decreases, $f_c(1 - f_v)$ increases and $f_v(1 - f_c)$ decreases. Hence the gain [which depends on $f_c(1 - f_v) - f_v(1 - f_c)$, see

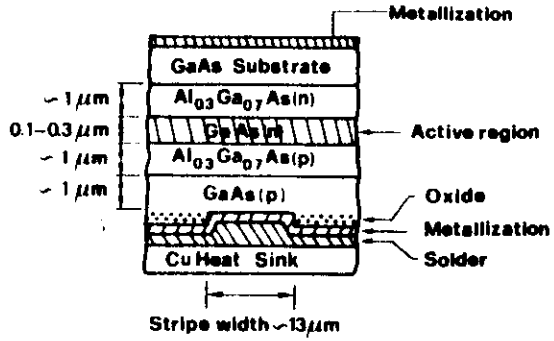

FIG. 6.33 Schematic diagram of a double-heterojunction semiconductor laser. The active region consists of the GaAs(n) layer (hatched area).

equation (6.26)] increases rapidly. As a consequence of this, homojunction lasers can operate cw only at cryogenic temperatures. This constitutes a serious limitation of this type of laser.

To overcome this difficulty, heterojunction lasers have been used. Figure 6.33 shows an example of a double heterojunction GaAs laser. In this diode there are two junctions [$Al_{0.3}Ga_{0.7}As(p)$–GaAs and GaAs–$Al_{0.3}Ga_{0.7}(n)$] between different materials. The active region consists of a thin layer of GaAs (0.1–0.3 μm). With such a diode, the threshold current density for room-temperature operation can be reduced by about two orders of magnitude (i.e., to $\sim 10^3$ A/cm^2) compared with the homojunction device. Thus cw operation at room temperature is made possible. The reduction of threshold current density is due to the combined effect of three circumstances: (i) The refractive index of GaAs ($n \simeq 3.6$) is significantly larger than that of $Al_{0.3}Ga_{0.7}As$ ($n \simeq 3.4$), thus providing an optical-waveguide structure. This means that the laser mode will now be confined in the GaAs layer, i.e., in the region where the gain is, and, unlike the situation in the homojunction diode, the wings of the field distribution no longer extend into the unpumped (and therefore absorbing) regions. (ii) The band gap of $Al_{0.3}Ga_{0.7}As$ (~1.8 eV) is significantly larger than that of GaAs (~1.5 eV). Energy barriers are therefore formed at the two junctions which effectively confine injected holes and electrons in the active layer (Fig. 6.34). For a given current density, the concentration of holes and electrons in the active layer is thus increased, and therefore the gain is also increased. (iii) The heat dissipation capability of the diode has been considerably improved. This has been achieved by cementing the GaAs(p) substrate to a copper (or tin) plate which, because of its mass and thermal conductivity, acts as a heat sink.

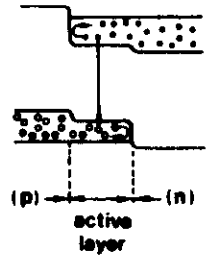

FIG. 6.34. Energy band diagram of a double-heterostructure semiconductor laser.

Semiconductor lasers cover a broad wavelength range from around 0.7 to ~30 μm. At present the most important semiconductor laser is perhaps the GaAs laser ($\lambda = 0.84$ μm). Continuous output powers up to a few milliwatts (5–10 mW) at room temperature with an overall slope efficiency of about 10% have been obtained. The internal quantum efficiency (fraction of injected carriers which recombine radiatively) is even higher (~70%). Semiconductor lasers are therefore among the most efficient of lasers. We note that, due to the large oscillation bandwidth ($\sim 10^{11}$ Hz for GaAs), the possibilities for mode-locked operation are attractive. Pulses of about 5 ps duration have indeed been obtained with passively mode-locked GaAs lasers. Note also that ternary compounds such as $Ga(As_{1-x}P_x)$ can also be used. The oscillating wavelength ranges from $\lambda = 0.84$ ($x = 0$) to 0.64 μm ($x = 0.4$). Thus, by varying the composition, it is possible to continuously vary the output wavelength. Gallium arsenide lasers are attractive as sources in optical communication links using optical fibers as the transmitting medium. Operating lifetimes in excess of 10^6 h have already been demonstrated with double-heterojunction GaAs lasers. The GaAs laser is also very interesting in a number of applications requiring only a low-power laser (such as optical reading) where it is no disadvantage to use infrared rather than visible light. Double-heterojunction semiconductor lasers operating at either $\lambda \simeq 1.3$ or $\lambda \simeq 1.6$ μm, where two minima for the loss of a quartz optical fiber occur, are now being vigorously developed. Here, the most interesting semiconductor for the active region seems to be the quaternary alloy $In_{1-x}Ga_xAs_yP_{1-y}$, while the p and n sides of the junctions may be made of the simple binary compound InP. If $y = 2.2x$, the quaternary alloy is lattice matched to InP, and by the appropriate choice of x the emission wavelength can be tuned from 0.92 to 1.5 μm.

Of the various other semiconductor lasers, mention should be made of the lead salt lasers,[38] all oscillating in the middle-to-far infrared, and in particular the ternary compounds $PbS_{1-x}Se_x$(4–8.5 μm), $Pb_{1-x}Sn_xTe$(6.5–32 μm), and $Pb_{1-x}Sn_xSe$(9–30 μm). Laser operation in these cases requires cryogenic temperatures ($T \simeq 77$°K for cw operation). For a given index of

composition x, the wavelength of the emitted radiation can be tuned by applying a magnetic field, by applying hydrostatic pressure, or by changing the diode current (heating effect). Typical applications of these lead salt lasers are found in the field of infrared spectroscopy, particularly in high-resolution spectroscopy. The linewidth of the emitted radiation can indeed be made very narrow (e.g., ~50 kHz for PbSnTe).

6.7 COLOR-CENTER LASERS[32]

A number of different types of color centers in alkali halide crystals are now being used as the basis of efficient, optically pumped lasers with broad tunability in the near infrared. At present color-center lasers allow operation over the wavelength range 0.8–3.3 μm. On a scale of increasing wavelength, these lasers thus take over just where the organic dyes give up.

Figure 6.35 indicates the structure of some color centers which are of interest to the present discussion. Of these only the F_A and F_2^+ centers have been made to lase. The ordinary F center can be regarded as an archetype of the other varieties of F-like centers: It consists of an electron trapped in an anion vacancy of the crystal. On the other hand, if one of the six metal ions immediately surrounding the vacancy is foreign (indicated by the smaller circle in the figure; e.g., Li^+ in a potassium halide), the defect is known as an F_A center. Two adjacent F centers along a (110) direction constitute a so-called F_2 center, and F_2^+ is its singly ionized counterpart. The general energy level scheme of an F center is shown in Fig. 6.36. After

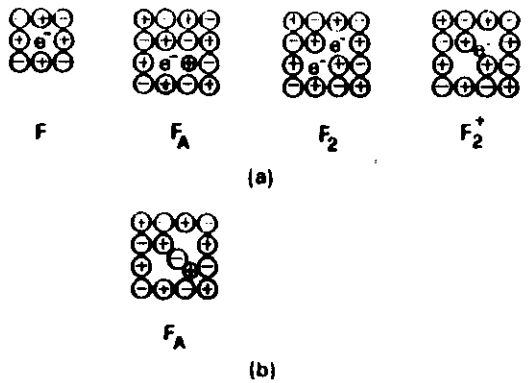

FIG. 6.35. (a) Normal structure of F, F_A, F_2, and F_2^+ color centers. (b) Relaxed structure of the F_A center. The electron (not shown) shares the two empty spaces of the lattice.

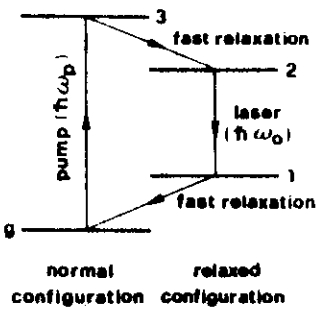

FIG. 6.36. The pumping cycle of an F-center laser.

it has been raised to its excited state 3, the F center rapidly (of the order of picoseconds) relaxes to its state 2. The configuration of this so-called relaxed state is also indicated in Fig. 6.35 for the F_A center. Relaxation consists of a simple expansion of the vacancy (or of the double vacancy) for F, F_2, and F_2^+ centers. The F center then decays (radiatively) to its relaxed ground state (state 1 in Fig. 6.36) and then from there it rapidly decays to the unrelaxed ground state g. Since both the excitation ($g \rightarrow 3$) and emission ($2 \rightarrow 1$) transitions are rather broad (~4000 Å), these spectra are reminiscent of dye lasers (see Fig. 6.22), the emission spectrum being Stokes shifted relative to the absorption spectrum. F centers are thus seen to fulfill the requirement of a four-level laser rather well. Not all F centers are good candidates for laser action, however, since some of them (e.g., the ordinary F center) have a very low fluorescence quantum efficiency. Of the F_A-type lasers, we mention the KCl:Li ($\lambda = 2.5$–2.9 μm) and RbCl:Li ($\lambda = 2.7$–3.3 μm) lasers. Of the F_2^+-type lasers we mention the NaF ($\lambda = 0.88$–1 μm), KF ($\lambda = 1.25$–1.45 μm), and LiF ($\lambda = 0.84$–1.04 μm) lasers. It should be noted that the preparation of laser crystals based on these F_A and F_2^+ types of color centers requires considerable care and skill.

Figure 6.37 illustrates the sort of layout used in a color-center laser. The laser is longitudinally pumped by another laser (usually a Kr^+ laser oscillating on its red, 647 nm, transition or a Nd:YAG laser) in a configuration similar to that used for cw dye lasers (compare with Fig. 6.25b). Here the pump beam passes through the input mirror, which has a high reflectivity at the laser wavelength and a high transmission at the pump wavelength. Coarse tuning of the laser is usually achieved by means of a dispersive optical system such as a prism or a grating (they are not included in Fig. 6.37; however, see Fig. 5.7). The fine tuning and selection of a single mode is achieved by using one or more Fabry-Perot etalons in the cavity (see Fig. 5.8). A complicating feature of color-center lasers is the need to keep the laser crystal at cryogenic temperatures (usually $T \simeq 77°K$). There are

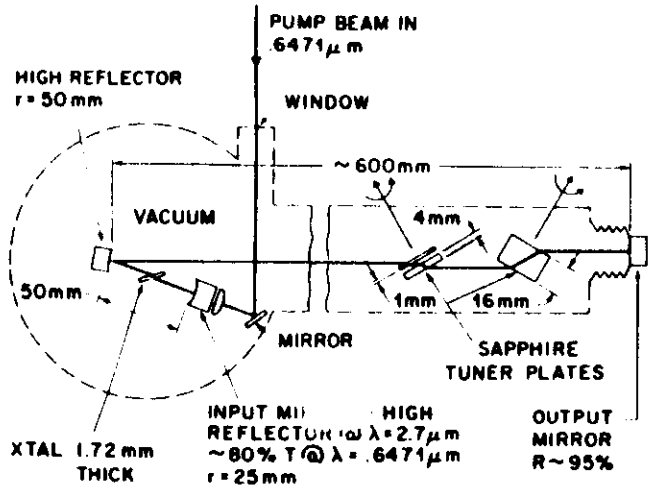

FIG. 6.37. Typical layout of a cw color-center laser. The data indicated in the figure refer to a KCl:Li laser longitudinally pumped by a Kr^+ laser [after Mollenauer[32]].

two reasons for this: (i) The lifetime τ of the upper laser level decreases roughly as $1/T$ for the F_A center. Thus the laser threshold [$\propto 1/\sigma\tau$, see (6.12)] is expected to increase linearly with T. (ii) Both F_A and F_2^+ centers fade (in ~1 day) if the temperature is increased beyond ~200°K. This last point poses a problem as far as the shelf life of color-center lasers is concerned.[†] Note finally that the whole laser cavity is usually kept in a vacuum enclosure (dashed line in Fig. 6.37) for two reasons: (i) on account of the low temperature requirement of the laser crystal, and (ii) to prevent losses due to atmospheric absorption (especially by H_2O) from interfering with laser action.

The performance of color-center lasers can be summarized as follows. Typical threshold pump powers are of the order of a few tens of milliwatts (when the pump beam is focused down to a 20-μm-diameter spot in the crystal). Continuous wave output powers up to 1 W with slope efficiency up to 7% for F_A and up to 60% for F_2^+ have been obtained. The difference of almost an order of magnitude in slope efficiency between the two types of laser requires a comment. It arises from the fact that the pump quantum efficiency ($\hbar\omega_0/\hbar\omega_p$, see Fig. 6.36) is ~80% for F_2^+ centers while it is only ~10% for F_A centers. The slope efficiency in this case is essentially determined by the quantum efficiency since the slope efficiency is the

[†]Some new classes of color-center lasers (e.g., Tl^+-doped alkali halides) have recently been shown to be both optically and thermally stable, however.

product of pump quantum efficiency and coupling efficiency [see (5.24b)] if we assume $\eta_p = 1$ (all pump photons absorbed) and $\eta_d = 1$ (in view of the very fast decay of the lower laser level). We finally note that some color-center lasers (LiF and KF, F_2^+ centers) have also been mode locked using the same technique of synchronous pumping as for dye lasers. Pulses as short as 5 ps and tunable over the laser's emission range have been obtained in this way.

By virtue of their broad tunability, their very narrow oscillation linewidth, and their picosecond pulse capabilities, color-center lasers look very interesting for applications in many areas such as molecular spectroscopy, chemical dynamics, and evaluation of optical fibers.

6.8 THE FREE-ELECTRON LASER[33]

In the previous sections our discussion has progressed from situations in which electrons are bound to a single atom or molecule, to situations in which the electron is free to move along the chain of atoms in a conjugated double-bonded molecule (dye lasers), and then to situations in which the electron is free to move through the entire volume of a semiconductor crystal (semiconductor lasers). In this last topic of the chapter, we describe one of the most recent and interesting types of laser, in which the electrons are even more free than in the cases considered so far: the free-electron laser. In fact in this laser the electrons move freely (they are in a vacuum) through a periodic magnetic field and the stimulated emission process comes about through the interaction of the e.m. field of the laser beam with the electrons moving in this periodic structure. Free-electron lasers can in principle generate stimulated radiation of high peak intensity (~a few MW/cm^2) at any wavelength from the IR to the UV and perhaps even in the x-ray region of the e.m. spectrum. So far, however, this type of laser has only been operated at $\lambda = 3.4$ μm.[34]

A schematic diagram of a free-electron laser is shown in Fig. 6.38. A beam of relativistic electrons is passed through a periodic transverse magnetic field (the "wiggler"). Stimulated emission along the direction of the

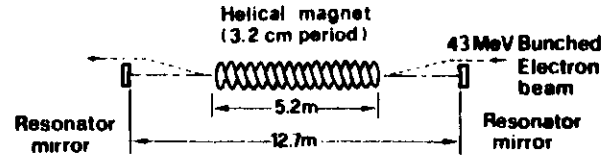

FIG. 6.38. Schematic diagram of a free-electron laser [after Deacon *et al.*[34]].

electron beam is fed back, just as in any other laser, by means of two mirrors of appropriate reflectivity. The stimulated emission process has its origin in the interaction of the e.m. wave with the electrons moving in the periodic magnetic structure. This effect may be properly termed magnetic bremsstrahlung. Radiation can also be absorbed through the process of inverse bremsstrahlung. The wavelengths for emission (plus sign) and absorption (minus sign) are given by[35]

$$\lambda = \frac{\lambda_q}{2\gamma^2}\left[1 + \left(\frac{1}{2\pi}\right)^2 \frac{\lambda_q^2 r_0}{mc^2} B^2\right]\left(1 \pm \frac{h\nu}{\gamma mc^2}\right) \tag{6.29}$$

where λ_q is the period of the magnetic field, γmc^2 is the electron energy (ergs), m is the electron mass, r_0 is the classical electron radius (cm), and B is the transverse magnetic field. Since the emission wavelength is slightly longer than that for absorption, one observes gain on the long-wavelength side and loss on the short-wavelength side of the transition. The minimum theoretical value for the linewidth arises from spontaneous emission and is determined by the length of the magnet assembly. There are also inhomogeneous effects, however, arising, for instance, from the spread in electron energy, the angular divergence of the electron beam, and the variation in magnetic field over the cross section of the beam.

With the arrangement shown in Fig. 6.38, laser action has been obtained at $\lambda \simeq 3.4$ μm with an average output power of 0.36 W and peak power (the e beam was pulsed) of 7 kW. The light was circularly polarized with the same polarization as the helical magnet.

From (6.29) it is seen that the transition wavelength can be varied by changing the electron energy and/or the magnet period. Since, however, the gain of the transition scales as $\lambda^{3/2}J$,[35] where J is the e-beam current density, it follows that higher electron beam currents will be required for laser operation in the visible and ultraviolet. The facilities afforded by present-day e-beam machines offer the possibility of producing laser action to wavelengths at least as short as 100 nm. The need for a sophisticated e-beam machine and the relatively low efficiency of this laser ($< 0.5\%$) seem at present to be the most serious limitations. The future of free-electron lasers appears therefore to be dependent on the development of relatively large national facilities.

6.9 SUMMARY OF PERFORMANCE DATA

By way of a summary, a selection of the laser performance data given in the previous sections has been gathered together in Table 6.1. Although

TABLE 6.1. Performance Data of Some of the Lasers Described in This Chapter

Laser type	Mode of operation[a]	λ, nm	Average power, W	Peak power, kW	Pulse duration	Slope efficiency, %
Ruby	P	694.3	1	10–10^4	1 ms–10 ns	< 0.1
Nd:YAG	cw	1064	150			1–3
Nd:YAG	P	1064	400	10	1–5 ms	1–3
Nd:YAG	P	1064	4	2×10^4	10–20 ns	1–3
He–Ne	cw	632.8	10^{-3}–10^{-2}			
Cu	P	510.5	40	100	20–40 ns	1
Ar^+	cw	514.5	10–150			< 0.1
He–Cd	cw	325 441.6	0.1			
CO_2	cw	10.6 μm	$(1–15) \times 10^3$			10–20
CO_2	P	10.6 μm	10^3	10^4	0.1–0.5 μs	10
N_2	P	337.1	0.1	10^3	10 ns	< 0.1
KrF	P	248	100	5×10^3	10 ns	1
Rhodamine 6G	P	590	100	100	10 μs	0.5
HF	cw	2.6–3.3 μm	10^4			
HF	P	2.6–3.3 μm		10^3		
GaAs	cw	840	10^{-2}			10

[a] P = pulsed; cw = continuous wave.

the list of lasers covered in Table 6.1 is already quite numerous, it must be realized that this only represents a tiny fraction of the lasers that have been operated so far. By way of an illustration of this, Fig. 6.39 shows the wavelength ranges over which the various types of lasers have actually been operated. The same figure also shows the potential ranges for the three different types of gas-laser transitions which can be used: (i) transitions between electronic state, (ii) vibrational–rotational transitions, and (iii) rotational transitions. However, it should be noted that these ranges cannot, in general, be covered continuously by existing lasers. Dye lasers and color-center lasers, however, are exceptions to this, and the ranges shown for them can be covered continuously.

The wide range of wavelengths which can now be covered with lasers is worth emphasizing (roughly 0.1 to 10^3 μm, i.e., a factor of 10^4 between the extremes of the range). Besides the wavelength, there are other laser parameters which can span a wide range. In fact we have seen that the output power ranges from the milliwatt level of low-power cw lasers up to 100 kW (and possibly much more, but this information is classified) for high-power cw lasers and up to 100 TW for pulsed lasers. Likewise, laser pulsewidths can range from milliseconds (for pulsed solid-state lasers) to

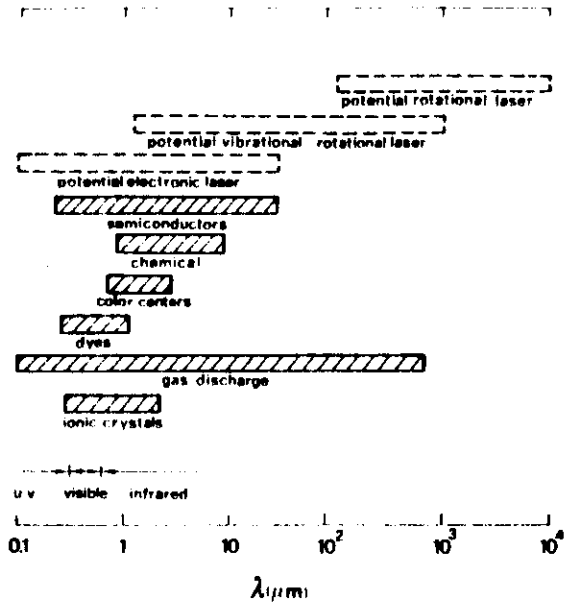

FIG. 6.39. Wavelength ranges for existing lasers in six of the categories considered in the text. The figure also shows the potential ranges for the three types of transitions used in gas lasers.

picoseconds (for mode-locked lasers). The physical dimensions of different types of laser also cover an extraordinary range: this goes from a few micrometers to a few tens of meters (one of the longest lasers was used for geodesic studies and had a length of 6.5 km!). This enormous variety of laser types and laser performance parameters is perhaps one of the most fascinating features of the laser field. It also means that, with such a range of lasers available, there is a considerable variety of applications, and these will be discussed at some length in Chapter 9.

PROBLEMS

6.1. Draw a scale covering the wavelength range of visible e.m. waves. Where do ruby, He–Ne, Ar^+, and Rhodamine 6G lasers fall within this range? What is the corresponding color of the emitted light?

6.2. List at least four lasers whose wavelengths fall in the infrared.

6.3. List at least three lasers whose wavelengths fall in the UV or VUV. What are the problems in getting laser action in the UV or VUV?

6.4. Estimate the width of the Lamb dip for a red He–Ne laser. Compare this with the Doppler width.

6.5. Estimate the width of the Lamb dip for an Ar^+ laser and compare it with the Doppler width.

6.6. Estimate the width of the Lamb dip for a longitudinal-flow CO_2 laser and compare it with the Doppler width.

6.7. For possible surgical applications, a laser with cw output power > 20 W is needed. What lasers satisfy this condition?

6.8. For metalworking applications, a laser with cw output power > 1 kW is needed. Which lasers meet this requirement?

6.9. Assume that the bond between the two nitrogen atoms of the N_2 molecule can be simulated by a spring of suitable elastic constant. Knowing the vibrational frequency (Fig. 6.10) and the atomic mass, calculate the elastic constant. Compare this constant with that obtainable from the ground-state curve of Fig. 6.19.

6.10. Assume that each of the two oxygen–carbon bonds of the CO_2 molecule can be simulated by a spring with force constant k_1. Calculate this constant from a knowledge of the ν_1 frequency (assume $\nu_1 = 1337\ cm^{-1}$). With the further assumption that there is no interaction between the two oxygen atoms, calculate the expected frequency ν_3 of the asymmetric stretching mode.

6.11. Show that the bonds of the CO_2 molecule cannot be simulated by elastic springs connecting the three atoms if the harmonic oscillation corresponding to the bending mode of frequency ν_2 has to be calculated.

6.12. Show that, if the elastic constant of the N–N bond is taken to be the same as that of the isoelectronic CO molecule, the $(v' = 1) \rightarrow (v = 0)$ transition wavelength of the N_2 molecule is approximately the same as that of the CO molecule.

6.13. From the knowledge that the maximum population of the upper laser level of a CO_2 molecule occurs for the rotational quantum number $J' = 21$ (see Fig. 6.13), calculate the rotational constant B [assume $T = 400°K$, which corresponds to an energy kT such that the corresponding frequency (kT/h) is $\sim 280\ cm^{-1}$].

6.14. Using the result of the previous problem, calculate the frequency spacing (in cm^{-1}) between the rotational lines of the CO_2 laser transition (assume that the rotational constant of the lower laser level is the same as that of the upper laser level, and remember that only levels with odd values of J are occupied).

6.15. The collision broadening of the CO_2 laser transition is $\Delta\nu_c = 7.58\ (\psi_{CO_2} + 0.73\psi_{N_2} + 0.6\psi_{He})p(300/T)^{1/2}$ MHz, where the ψ are the fractional partial pressures of the gas mixture and p is the total pressure (Torr). If the ratio of partial pressures of CO_2, N_2, and He molecules is 1:1:8, calculate the total gas pressure needed to make all the rotational lines merge together. What would the width of the gain curve then be?

6.16. If a CO_2 laser with high enough pressure to have all its rotational lines merged together were mode locked, what would be the order of magnitude of the corresponding laser pulse width?

REFERENCES

1. V. Evthuhov and J. K. Neeland, in *Lasers*, ed. by A. K. Levine (Marcel Dekker, New York, 1966), Vol. 1, Chapter 1.
2. T. H. Maiman, *Nature* **187**, 493 (1960).
3. T. H. Maiman, *Br. Commun. Electron.* **7**, 674 (1960).
4. D. Findlay and D. W. Goodwin, in *Advances in Quantum Electronics*, ed. by D. W. Goodwin (Academic Press, New York, 1970), pp. 77–128.
5. H. G. Danielmeyer, in *Lasers*, ed. by A. K. Levine and A. J. DeMaria (Marcel Dekker, New York, 1976), Vol. 4, Chapter 1.
6. W. Koechner, *Solid State Laser Engineering* (Springer Verlag, New York, 1976), Chapter 2.
7. A. Javan, W. R. Bennett, and D. R. Herriott, *Phys. Rev. Lett.* **6**, 106 (1961).
8. C. S. Willet, *An Introduction to Gas Lasers: Population Inversion Mechanisms* (Pergamon Press, Oxford, 1974), Chapter 4, Section 4.1.1.
9. R. Arrathoon, in *Lasers*, ed. by A. K. Levine and A. J. De Maria (Marcel Dekker, New York, 1976), Vol. 4, Chapter 3.
10. W. B. Bridges, in *Methods of Experimental Physics*, Vol. 15, *Quantum Electronics*, ed. by C. L. Tang (Academic Press, New York, 1979), Part A, pp. 33–151.
11. C. C. Davis and T. A. King, in *Advances in Quantum Electronics* ed. by D. W. Goodwin (Academic Press, New York, 1975), Vol. 3 pp. 170–437.
12. M. H. Dunn and J. N. Ross, in *Progress in Quantum Electronics*, ed. by J. H. Sanders and S. Stenholm (Pergamon Press, London, 1977), Vol. 4, pp. 233–270.
13. Y. Y. Chang, in *Nonlinear Infrared Generation*, ed. by Y. R. Shen (Springer-Verlag, Berlin, 1977), Chapter 6.
14. P. K. Cheo in *Lasers* ed. by A. K. Levine and A. J. De Maria (Marcel Dekker, New York, 1974), Vol. 3, Chapter 2.
15. A. J. De Maria, in *Principles of Laser Plasmas*, ed. by G. Bekefi (Wiley-Interscience, New York, 1976), Chapter 8.
16. C. K. N. Patel, *Phys. Rev. Lett.* **12**, 588 (1964).
17. R. L. Abrams, in *Laser Handbook*, ed. by M. L. Stitch (North Holland, Amsterdam, 1979), Vol. 3, Part 2A.
18. O. R. Wood, *Proc. IEEE* **62**, 355 (1974).
19. J. D. Anderson, *Gasdynamic Lasers: An Introduction* (Academic Press, New York, 1971).
20. M. L. Bhaumik, in *High-Power Gas Lasers*, ed. by E. R. Pike (The Institute of Physics, Bristol and London, 1975), pp. 122–147.
21. C. S. Willet, *An Introduction to Gas Lasers: Population Inversion Mechanisms* (Pergamon Press, Oxford, 1974), Sections 6.2.1 and 6.2.3.
22. C. A. Brau, in *Excimer Lasers*, ed. by C. K. Rhodes (Springer-Verlag, Berlin, 1979), Part 4.
23. F. P. Schäfer, in *Dye Lasers*, 2nd edn. ed. by F. P. Schäfer (Springer-Verlag, Berlin, 1977).
24. O. G. Peterson, in *Methods of Experimental Physics*, Vol. 15, ed. by C. L. Tang (Academic Press, New York, 1979), Part A, pp. 251–355.
25. P. P. Sorokin and J. R. Lankard, *IBM J. Res. Dev.* **10**, 162 (1966).
26. A. N. Chester, in *High-Power Gas Lasers*, ed. by E. R. Pike (The Institute of Physics, Bristol and London, 1975) pp. 162–221.

27. C. J. Ultee, in *Laser Handbook*, Vol. 3, ed. by M. L. Stitch (North-Holland, Amsterdam, 1979), pp. 199–287.
28. K. Hohla and K. L. Kompa, in *Handbook of Chemical Lasers*, ed. by R. W. F. Gross and J. F. Bott (John Wiley and Sons, New York, 1976), pp. 667–702.
29. H. Kressel, in *Methods of Experimental Physics*, Vol. 15, ed. by C. L. Tang (Academic Press, New York, 1979), Part A, pp. 209–250.
30. R. N. Hall *et al.*, *Phys. Rev. Lett.* **9**, 366 (1962).
31. M. I. Nathan *et al.*, *Appl. Phys. Lett.* **1**, 62 (1962).
32. L. F. Mollenauer, in *Methods of Experimental Physics*, Vol. 15, ed. by C. L. Tang (Academic Press, New York, 1979), Part B, pp. 1–54.
33. *Physics of Quantum Electronics*, Vol. 7, ed. by W. Lamb, M. Sargent, and M. Scully (Benjamin, New York, 1980).
34. D. A. G. Deacon *et al.*, *Phys. Rev. Lett.* **38**, 892 (1977).
35. L. Elias *et al.*, *Phys. Rev. Lett.* **36**, 717 (1976).
36. H. D. Forsterling and H. Kuhn, *Physikalische Chemie in Experimenten*, Ein Praktikum (Verlag Chemie, Weinheim/Bergstr., 1971).
37. J. D. Daugherty, in *Principles of Laser Plasmas*, ed. by G. Bekefi (John Wiley and Sons, New York, 1976), pp. 369–419.
38. I. Melngailis and A. Mooradian, in *Laser Applications in Optics and Spectroscopy*, ed. by S. Jacobs, M. Sargent, M. Scully, and J. Scott, (Addison-Wesley Company, 1975).
39. M. C. Richardson *et al.*, *IEEE J. Quantum Electr.* **QE-9**, 236 (1973).